Bow River Fish Population Assessment

1999-2023 Final Report

JANUARY 2025

Classification: Public

Bow River Fish Population Assessment 1999-2023 Final Report | Environment and Protected Areas

Prepared by: Dr. Josh Korman, Ecometric Research, Vancouver, BC

Prepared for: Environment and Protected Areas, Fish and Wildlife Stewardship Branch, Cochrane AB

Contents

Abstract

The abundance of non-native, self-reproducing Rainbow Trout (*Oncorhynchus mykiss*) and other sportfish in the lower Bow River has been monitored for more than two decades using boat electrofishing. To date, models that estimate abundance have been based on multi-pass mark-recapture data and have not made use of additional data from locations that were sampled using only a single pass of electrofishing effort. This report describes a Bayesian closed-population model to estimate abundance of Rainbow Trout by size class using boat electrofishing survey data collected between 1999 and 2021. Unlike previous efforts, this model integrates data from both mark-recapture and one-pass sampling to estimate annual abundance. The model is also unique in that it estimates capture probability and abundance at the site level, and then aggregates the estimates to produce an annual estimate, thus avoiding bias due to heterogeneity in capture probability across sites. The model explicitly accounts for the effects of fish size, year, site, and pass on capture probability, and potential mark loss from sampling sites resulting from the movement of tagged fish. The model can easily be applied to other species that have been marked as part of the Bow River program, such as Brown Trout and Mountain Whitefish.

Capture probability of Rainbow Trout was very dependent on fish size, ranging from ~ 1-3% for the smaller size classes (≤ 200, 200-250, 250-300 mm) to ~ 9% for the largest (≥ 500 mm). Year was also an important determinant of capture probability. For example, the capture probability for the most dominant size class (400-500 mm) ranged from a low of ~4% in 2001 to a high of 13% in 2021. Year effects on capture probability were generally well-determined in years when mark-recapture sampling was implemented and more uncertain in years when only one-pass sampling was done. Capture probabilities from more recent years of sampling with mark-recapture data (2018 and especially 2021) were both higher and more precise compared to earlier years, leading to substantial improvements in the precision of annual abundance estimates. The effect of sampling site on capture probability was poorly determined because the number of recaptures within sites was generally low. Previously captured fish, at large for 1-4 days prior to a second capture, had capture probabilities that were 1.7-fold higher than those for unmarked fish that had not been previously captured within annual surveys. It is possible that this potential 'trap-happy' response was caused by capture-handling-release effects which did not dissipate over the short period between passes. However, this effect was uncertain and challenging to estimate owing to overall low capture probabilities and limited depletion of the unmarked population across passes.

The average of annual abundance estimates for Rainbow Trout between 1999 and 2021 was 683 fish/km (all size classes combined), with an average coefficient of variation of annual estimates of ~0.30. The population declined at a rate of ~3%/year (95% credible interval of -6.1% - -0.1%). This rate of decline is slower than the mean estimate from Cahill et al. (2018) for the 2003-2013 period of ~ 6%. The difference in estimates between studies is likely due to a combination of differences in model structure, input data, and the period of evaluation (1999-2021 for the trend presented here, vs. 2003-2013 used in Cahill et al.). This analysis indicates there is substantive year-to-year variation in abundance around the declining trend. Thus, the trend is a poor predictor of abundance in any particular future year. Model results are used to provide a series of recommendations for future sampling and analysis.

Von Bertalanffy growth models fit the Bow River Rainbow Trout length-at-age data well and predicted asymptotic sizes ranging from ~520 – 640 mm across years. Length-at-age was substantively lower in 2012 and 2013, at intermediate levels in 2017 and 2021, and higher in other years (1999-2001, 2003,

2005, 2011, 2014). Although there was substantive overlap in size ranges among adjacent ages, especially for older fish, von Bertalanffy models were effectively used to convert abundance by size class into abundance by age class. Preliminary analyses indicate scale-based ages relative to otolith ages are not biased, however the sample size for comparison is small. The resulting multi-year time series of abundance by age class can be used to provide insights about population dynamics. Given strong evidence that length-at-age has varied across years, continuation of age sampling is warranted. Sample sizes in 2014 and later years, when age determinations were largely made using otoliths, have been small. Small sample size results in greater uncertainty in von Bertalanffy models, and hence greater uncertainty in translation of size- to age-based abundance. Thus, increasing the annual sample size of scale-based age estimates is recommended. A size-stratified age sampling design would ensure there are sufficient samples across the full range of size classes, which in turn will lead to greater certainty in estimated length-at-age relationships. Given the small sample size of individuals aged by both otolith and scales, a small size-stratified sample of individual fish aged by both methods each year is recommended. These data will contribute to a more robust determination of the accuracy of scale-based age estimates than presented here and can also be used to verify that annual age estimates continue to be accurate.

1.0 Introduction

The lower Bow River supports an important sport fishery for Rainbow Trout, Brown Trout, and Mountain Whitefish (Cahill et al. 2018). The abundance of these populations has been monitored for more than two decades to assess population trends and inform management decisions. Data from multi-pass mark-recapture boat electrofishing sampling at discrete sites are used to estimate abundance. Data from one-pass surveys at discrete sites are used to increase the spatial coverage of sampling to make broader inferences about the state of the populations, but that data has not been used to estimate abundance to date.

To determine trends in the abundance and size structure of the sportfish populations in the Bow River, modelling is required to convert catch and mark-recapture data into estimates of size-specific abundance. A variety of methods, applied to different portions of the long-term dataset, have been used (e.g., Henderson, 2013; Cahill et al. 2018). This report describes a new Bayesian closed population model to estimate abundance of Rainbow Trout based on available mark-recapture and one-pass data collected between 1999 and 2021. The model can be applied to other species that have been marked, such as Brown Trout and Mountain Whitefish. Unlike previous efforts, this model integrates data from both mark-recapture and one-pass sampling to estimate annual abundance. The model is also unique because it estimates capture probability and abundance at the site level, and then aggregates the abundance estimates across sites sampled in a year to produce an annual estimate. Further, the model explicitly accounts for the effects of fish size, year, site, and pass on capture probability, and can therefore better inform decisions about future monitoring.

Aging data from lower Bow River fish populations are used to describe the relationship between fish age and size which has two very practical applications. First, models fit to the age-length data can be examined to determine if there are interannual trends in growth rates. Growth rates can drive important population-level processes for Rainbow Trout such as maturation, fecundity, recruitment, and even survival rates of mature fish (Korman et al. 2017, 2021). Changes in growth are often easier to detect and attribute to abiotic or biotic drivers. Second, length-at-age data and models can be used to estimate the proportions of different ages within size classes. This allows conversion of abundance estimates by size class into abundance estimates by age class, which facilitates calculation of key processes influencing population dynamices, like recruitment and survival rate.

This report describes the models that were developed (section 2.0), and applies them to the Rainbow Trout data from the Bow River collected between 1999 and 2021 (section 3.0). Key aspects of the data and modelling results are summarized, and recommendations for consideration in future monitoring and modelling are provided (section 4.0). The report also includes an appendix that describes the workflow to generate model input files, run the model, and summarize the output (appendix A.1).

2.0 Methods

2.1 Electrofishing Data and Survey Design

A closed population model was used to estimate the abundance of Rainbow Trout in the Bow River. The model can also be used to estimate abundance for other species captured by boat electrofishing and marked (e.g., Brown Trout and Mountain Whitefish). Annual surveys conducted in most years between 1999 and 2021, typically sampled both banks of multiple 1-kilomenter (km) long sites. The majority of survey years employed a mark-recapture approach where each site was sampled on multiple occasions (over consecutive days) within a year (Table 1). Fish were captured, enumerated, measured, and tagged based on a first pass of effort on day 1. The process was repeated on consecutive days for a total of typically four or five passes of effort. On each pass, unmarked fish can be caught, marked and released, and fish marked on previous passes can be recaptured. In the model these data are represented with the following symbols:

$\mathbf{u}_{y,s,p,l}$ the observed number of unmarked fish captured in year 'y' at site 's' on pass 'p' in size class 'l' (e.g., l = 1 for ≤200 mm fish, l = 2 for 201-250 mm fish, etc.)

$\mathbf{M}_{y,s,p,l}$ the number of marked fish released on pass 'p', which is the sum of unmarked fish given a new mark, and unique recaptures of previously marked fish on pass 'p'.

$\mathbf{r}_{y,s,p\_rel,p\_rec,l}$ the number of marked fish released on pass p_rel (new marks and unique recaptures) that are recaptured on pass p_rec.

In many years, the same four mark-recapture sites were sampled (Table 1). Mark-recapture sites were sampled with four or five passes over consecutive days in most years. A total of 94 mark-recapture experiments were conducted between 1999 and 2021 (unique year-site combinations), with approximately 50% conducted in 2001. In 1999 and 2000, sites were sampled two times per day. To be consistent with other years, the unmarked catch, unique marks, and unique recaptures across passes within a day in 1999 and 2000 were summed.

A site was considered a mark-recapture site if it was sampled with multiple passes on an annual survey, and at least one fish for the species being modelled was marked and measured (across all passes prior to the last one, i.e., there was an opportunity for recapture). If the site was sampled with multiple passes but no fish of the species being modelled were marked prior to the last pass, the site was treated as one-pass site, and only data from the first pass was used. For one-pass sites, only $u_{y,s,p}$=1,1 data are available to estimate abundance. In some years only data from mark-recapture sites were available, while in others, some sites were sampled using mark-recapture and others were sampled with a single pass of effort (2001, 2018 Table 1). In some years only data from one-pass sites are available (2017, 2019, 2020).

2.2 Closed Population Abundance Model

A closed population model was used to estimate the annual abundance of Rainbow Trout for six size classes (≤200 mm, 201-250 mm, 251-300 mm, 301-400 mm, 401-500 mm,>500 mm, Fig. 1) at each site that was sampled. Site-specific estimates were combined to estimate the annual abundance by size class and the total across size classes. The model uses a hierarchical Bayesian approach to increase the precision of abundance estimates at mark-recapture sites, and to estimate abundance at one-pass sites where capture probability cannot be directly estimated. The model accounts for mark loss at sites resulting from marked fish moving out of the site after initial marking and prior to potential recapture on latter passes.

I first describe the structure of the mark-recapture component of the model, and then describe how abundance at one-pass sites is estimated. Finally, I describe how estimates of abundance from mark-recapture and one-pass sites are combined to estimate annual abundance. In the equations which follow, Greek letters denote estimated parameters and bold Roman letters denote data. Non-bold Roman letters denote either subscripts for strata (i.e., year (y), site (s), pass (p), size class (l)), or state variables. State variables are not directly estimated and instead calculated based on data and/or parameter estimates.

2.2.1 Mark-Recapture Sub-Model

Capture probability (P) is defined as the proportion of fish at a sampling site that are captured by one pass of sampling effort. The logit of capture probability for each year (y), site (s), pass (p), and size class (l) is predicted using a linear mixed effects model,

1) $$logit(P_{y,s,p,l}) = \beta_l + \beta_p + \beta_s + \beta_y + \varepsilon_{y,s,p,l}$$

where β_l is a fixed effect predicting the capture probability (in logit space) for each size class 'l' on the first pass (p=1), β_p is a fixed effect predicting differences in capture probability on passes 2-5 relative to pass one (thus $\beta_{p=1}=0$). β_y and β_s are random effects predicting differences in capture probability across sites and years, respectively. $\varepsilon_{y,s,p,l}$ is a process error deviate drawn from a zero-centered normal distribution with a standard deviation σ_p ($\varepsilon_{y,s,p,l} \sim \text{norm}(0,\sigma\_p)$. Process error deviates account for unmodelled variation due to limitations in model structure. For example, the fixed effect β_p assumes that the pass effect on capture probability is consistent across all years, sites, and size classes. Similarly, the fixed effect of fish size (β_l) is assumed to be constant across years, sites, and passes. $\varepsilon_{y,s,p,l}$ deviates allow the model to more closely fit the data given such structural limitations. Random effects of year and site avoid negative bias in variance estimates due to pseudo-replication (Millar and Anderson 2004). For example, the year effect allows for the possibility that capture probabilities across all sites sampled in a year may not be independent due to a common year effect. This situation is no different from the typical description of

pseudo-replication in statistical texts, where for example individual plants in a plot are not independent samples owing to a shared plot effect.

The random effects of site on capture probabilities are assumed to arise from a zero-centered normal distribution,

2) $\beta_s \sim norm(0, \sigma\_s)$

with estimated standard deviation σ_s. Sites with higher-than-average capture probability will have values of $\beta_s>0$, while those with lower-than-average capture probabilities will have $\beta_s<0$. The precision of β_s estimates will be higher for sites with more recaptures and for sites that were repeatedly sampled across years.

Preliminary modelling indicated a strong temporal pattern in random year effects that may be caused by correlated variation in the skill and experience of boat operators and netters through time (i.e., the crew this year is somewhat similar to the crew last year and next year). The temporal pattern in annual capture probability deviates is accounted for by using a conditional autoregressive (CAR) model,

3) $\beta_y \sim car.norm(\boldsymbol{a_y}, \sigma\_y)$

where car.norm() represents a normal CAR model, and $\mathbf{a_y}$ is the adjacency vector for each year y. It specifies that the adjacent year for the first year being modelled is the following (2nd) year, and adjacent years for the second year are the previous year (1st), and following year (3rd), etc. For each year, the estimate of β_y is drawn from a normal distribution with a mean that is the average of estimates from the adjacent years (β_y-1 and β_y+1) and a standard deviation σ_y.

Parameters of the capture probability model are fit to the data based on the assumption that the observed number of recaptures is a random variable drawn from a binomial distribution (~binom()),

4) $\boldsymbol{r_{y,s,p\_rel,p\_rec,l}} \sim binom(P_{y,s,p,l} \cdot (1-\theta_y), \boldsymbol{M_{y,s,p_{rel},l}})$

where θ_y are estimates of the year-specific proportions of marked fish that leave sites after release and thus are unavailable for recapture in the same site on the following passes. Thus, P represents the capture probability of marked fish that have remained in the site they were marked in. The indices 'p_rel' and 'p_rec' represent the pass number that marks are released and recaptured on, respectively. Note this recapture likelihood can only be applied in cases when M is greater than zero. The number of cases where M=0 increases with the number of size classes that are modelled. Uncertainty in estimates of parameters defining P for any strata (y, s, p, l) will depend on the sample sizes M and r, with greater certainty (higher precision) when the number of marks or recaptures is larger[1]. An example of the data used in the recapture likelihood (eqn. 4) for a single year-site-size class is provided in Table 2.

[1] The binomial likelihood properly accounts for sampling error from two-outcome experiments, such as the flip of a coin (can only be a head or a tail), or a mark-recapture experiment (a marked fish is either recaptured or not recaptured). Sampling error must be accounted for when estimating parameters of the capture probability model owing to differences in the number of marked fish released and differences in capture probability. Using the coin-toss analogy, the probability of obtaining a head (0.5 for a balanced coin) will be more precisely determined if the number of coin tosses is large (n=100) compared to if the number of tosses is low (n=4).

The logit-transformed proportion of marked fish that move from the site they were marked into another location within the same sampling year is assumed to be a normally distributed random variable,

5) $logit(\theta_y) \sim norm(\mu\_\theta, \sigma\_\theta))$

where μ_θ and σ_θ are hyper-parameters which represent the mean and standard deviation of the hyper-distribution for θ_y. The year-specific logit proportions and their hyper-parameters are estimated from the binomial likelihood,

6) $\boldsymbol{r\_out_y} \sim binom\left(\theta_y, \boldsymbol{r\_out_y} + \boldsymbol{r_y}\right)$

where, **r_out** is the number of recaptures of fish that were marked in sites other than the ones they were recaptured in, and r represents total recaptures of fish marked and recaptured in the same site (the sum of the r's used in eqn. 4 across sites, passes and size classes). The ratio of $\mathbf{r_{out}}$ to the sum of $\mathbf{r_{out}}$ and **r** is the expected value of θ_y if all year-specific estimates are assumed to be independent (Table 3). The hierarchical structure used to estimate θ_y in the model (eqn. 5) assumes they are not independent and instead are draws from a normal distribution (in logit space). This approach improves the precision of θ_y in years when the sample sizes for r or rout are low (e.g., 1999 for RNTR, or for other species in most years, Table 3). Hierarchical Bayesian models are often described as a partial-pooling method because they find a happy medium between a pooled estimate (estimating a single value of θ for all years by combining data across years and therefore assuming no variation across years) and independent estimates (θ_y estimated for each year based on year-specific data only, the θ_y's in Table 3).

Abundance for a given year, site, and size class is estimated based on the estimated capture probability and a statistical comparison between observed and predicted catches of unmarked fish. The abundance of the unmarked population across passes is calculated from,

7a) $N_{y,s,l} = \exp(\nu_{y,s,l})$ transform log abundance estimate ν

7b) $U_{y,s,p,l} = N_{y,s,l}$ for p=1 (i.e., prior to pass 1)

7c) $U_{y,s,p,l} = U_{y,s,p-1,l} - NM_{y,s,p-1,l}$ for p = 2 – maximum number of passes

where $\nu_{y,s,l}$ is the estimated initial abundance in log space, N is the initial abundance, and NM is the number of marks applied. Logically, these equations predict that prior to pass 1, the abundance of unmarked population is equal to the abundance, as no fish have been marked. Prior to pass 2, the abundance of the unmarked population is simply the initial abundance less the number of fish known to have been given a mark on pass 1, etc.

The unmarked catch on each pass can then be predicted based on the estimated abundance of the unmarked population and capture probability,

8) $\hat{u}_{y,s,p,l} = U_{y,s,p,l} \cdot P_{y,s,p,l}$

where $\hat{u}$ is the prediction of the unmarked catch. Note the key assumption that capture probability of unmarked fish (P in eqn. 8) is the same as for previously marked fish (eqn. 4). As shown below, this

common but critical assumption of mark-recapture models can be relaxed by estimating different capture probabilities for these two groups of fish. Abundance is estimated based on a statistical comparison of predicted and observed unmarked catch via a Poisson likelihood,

9) $$u_{y,s,p,l} \sim pois(\hat{u}_{y,s,p,l})$$

Traditionally, the equivalent of a binomial likelihood (multinomial) is used in Jolly-Seber type mark-recapture models to estimate abundance (William et al. 2002). If this approach was used in the model, eqn. 9 would be replaced with $u_{y,s,p,l} \sim binom(P_{y,s,p,l}, U_{y,s,p,l})$. The binomial sampling distribution should be used if sampling without replacement across passes, while the Poisson distribution should be used when sampling with replacement across passes. If all fish are uniquely marked and do not lose their marks, then the binomial model (sampling without replacement) is the appropriate distribution because all unmarked fish captured on a pass must be different individuals compared to unmarked fish captured on earlier passes. However, in the case of the Bow River electrofishing data, on occasion some fish are captured but not marked prior to being released, and some fish may lose their marks after release. Thus, part of the unmarked population is sampled with replacement across passes, and there is some rationale for using the Poisson distribution. In addition, the Poisson likelihood is computationally more robust than the binomial, and does not require limits on the prediction of the unmarked population ($U_{y,s,p,l} \geq u_{y,s,p,l}$). Poisson and binomial likelihoods lead to similar levels of sampling uncertainty when capture probability is low or sample size (U in this case) is high (Hilborn and Mangel 1997). However, when these conditions are not met, say because U is small, the sampling error from the Poisson distribution will be higher. Both binomial and Poisson likelihoods assume that fish within a site are randomly distributed on each pass, when in fact they are very likely clumped. Clumping will lead to underestimation of sampling error for both binomial or Poisson likelihoods. Utilizing the Poisson likelihood, which admits slightly higher sampling uncertainty under some conditions compared to the binomial, is thus the lesser of two evils with respect to the assumption of random distribution.

A key assumption in the model described to this point is that the capture probabilities for marked and unmarked fish are equivalent. That is, the capture probability used to predict unmarked catch (eqn. 8) is the same capture probability used to predict recaptures of previously marked fish (eqn. 4). This assumption can be relaxed by estimating separate capture probabilities for previously marked and unmarked fish. In this case, eqn. 1 would be used to predict the capture probability for unmarked fish to predict unmarked catch (eqn. 8). The model predicting capture probability for previously marked fish (P_m) to predict the number of recaptures would now include one additional term (relative to eqn. 4), γ,

10) $$logit(P\_m_{y,s,p,l}) = \beta_l + \beta_p + \beta_s + \beta_y + \varepsilon_{y,s,p,l} + \gamma$$

where γ is an offset that represents the effect of previous capture (Williams et al. 2002). If γ is positive, capture probability for previously captured fish (i.e., marked fish) will be higher than for fish not previously caught (a trap-happy behavior). In contrast, if γ is negative, capture probability for a previously captured fish would be lower than for fish not previously caught (a trap-shy behavior). This model is often referred to as 'Mb' in the mark-recapture literature (Williams et al. 2002). The ability to reliably estimate γ depends on the extent to which the unmarked population at a site is depleted across passes, which provides a gross estimate of the capture probability for unmarked fish. If the capture probability is high, the depletion of the unmarked population over passes will be substantive. Further, if the population is large, all else being equal catches of unmarked fish will be higher, and there will be less uncertainty about the extent of

depletion resulting from sampling error. Under these conditions the depletion of the unmarked population across passes provides useful information to estimate γ. However, if the depletion of the population is limited, or the catch of unmarked fish is low, there will be high uncertainty in the estimate of γ and the model will struggle to distinguish between P and P_m. To aid the estimation I assumed that γ does not vary across years, sites, pass, and size classes.

2.2.2 One-Pass Sub-Model

Capture probability at sites sampled with only a single pass of effort cannot be estimated using only the data from these sites. However, estimates of parameters determining capture probability at mark-recapture sites can be used to simulate capture probabilities at one-pass sites to estimate abundance at the latter locations. To do this, the same estimates of the fixed effects of fish size and pass (eqn. 1) determined from mark-recapture sites are applied to the one-pass sites. If a one-pass site was sampled by mark-recapture in another year, the estimate of β_s is applied to that site, and if not, a random estimate of β_s is generated from the hyper-distribution (that would also be used for samples of β_s from other years). Similarly, if a one-pass site was sampled in a year when mark-recapture was done, the estimate of β_y is applied to the one-pass sites in that year. However, in years when only one-pass sites were sampled (2017, 2019, 2020, see Table 1), a random year effect is used based on random draws from the hyper-distribution. Recall the random year effect is based on an autoregressive model, so β_y values for 2017, 2019, and 2020 will be more similar to estimates from adjacent years (e.g., 2018, 2021). Random draws from the process error distribution will also be applied to each year-site-size class combination at one-pass sites. Owing to this approach, capture probabilities at one-pass sites will be more uncertain than at mark-recapture sites. The extent of the increase in uncertainty will depend on the magnitude of the variance terms that control across-year variation (σ_y), across-site variation (σ_s), and process error (σ_p).

Abundance at one-pass sites is calculated based on catch conditional on the simulated capture probability via,

11a) $$N_{y,s,l} = \frac{u_{y,s,p=1,l}}{P_{y,s,p=1,l}}.$$

An alternative formulation accounts for the sampling error of the unmarked catch at one-pass sites using,

11b) $$u_{y,s,l} \sim pois(P_{y,s,p=1,l} \cdot N_{y,s,l}).$$

Estimates of abundance from one-pass sites based on equation 11b were very slow to converge. This is not surprising for sites that were not sampled using mark-recapture over the entire study period. In these cases, estimates of β_s and ε would be largely confounded. If estimating abundance via eqn. 11b, as for

the mark-recapture model, uninformative normal priors on the log of abundance are used (see text below). One way to improve model convergence would be to assume that all site length-standardized abundance estimates (from mark-recapture and open sites) in each year arise from a common hyper-distribution. This approach would constrain the abundance estimates and likely improve the convergence at one-pass sites. However, this approach adds complexity to the model since the mean and variance of log-normal hyper-distributions of abundance for each study year would have to be estimated, which would be challenging in the many years when only four mark-recapture sites were sampled or when no mark-recapture sampling was done (Table 1). The limitation of the current approach that was used (eqn. 11a) is that the precision in abundance at low-density sites would be slightly overestimated. However, this would have a limited effect on the uncertainty in the annual abundance estimates.

2.2.3 Calculating Annual Abundance

The annual abundance for each year by size class is calculated by summing the site-specific abundance estimates and standardizing abundance to a fixed distance (1 km). In years with only mark-recapture data, the estimates of abundance across sites are summed and divided by the sum of the length of all sites (in kms) to provide an abundance estimate (per km). A similar approach is used to calculate abundance in years when only one-pass sites are sampled. In the years when data from both mark-recapture and one-pass sites are available, the total abundance across all sites is calculated and divided by the sum of the length of all sites. The total abundance across size classes, or for a group of size classes (e.g., > 250 mm) is calculated by summing the abundance across size classes.

The approach for aggregating size class and site abundance estimates will correctly propagate the uncertainty in size class- and site-specific estimates into annual estimates. The precision of the annual estimates will be higher for size class-aggregated estimates than size class-specific estimates. Similarly, the precision of annual estimates of abundance for a size class will be greater than the site-specific estimates. All else being equal, the precision of annual abundance estimates will increase with the number of sites sampled and will be higher in years when mark-recapture was done. The precision of annual abundance estimates is expected to be lowest in years with only one-pass data (e.g., 2017).

2.2.4 Prior Distributions and Implementation

Bayesian models require that prior distributions are specified for each parameter that is directly estimated. Uninformative prior distributions were used for all parameters in the base model to allow the data to drive capture probability and abundance estimates. The prior for the log of abundance for each year, site, and size class was an uninformative normal distribution with a mean of 6 (~ 400 fish/km) and a standard deviation (sd) of 1000. Uninformative gamma distributions (rate and shape parameters = 0.001) were used as the priors for the precision (1/variance) for all of the estimated standard deviations in the model. The priors for the mean of the normal distribution predicting the logit of year-specific movement rates of marked fish out of sites, and for fixed effects of fish size class and pass on capture probability,

were normal distributions with means of zero and standard deviations of 1000. As described below, the estimate the previous capture effect on capture probability (γ in eqn. 10) could not be reliably determined using an uninformative prior (sd=1000), and I therefore used a semi-informative normal prior (sd = 0.31) to explore the extent of evidence for trap-happy or trap-shy effects on capture probability and the resulting effects on abundance estimates. This prior limited the range of the previous capture effect (γ) to ± 1.25.

Posterior distributions were estimated by taking every 80th sample from a total of 100,000 MCMC (Markov chain Monte Carlo) simulations after excluding the first 20,000 'burn in' samples for each of 3 chains (total posterior sample size of 1,000 per chain or 3,000 across chains). This sample size and sampling strategy was sufficient to achieve adequate model convergence that was evaluated using the Gelman Rubin convergence diagnostic (Rhat<1.05). Run-time on a computer with an Intel-i7 CPE @ 2.90 GHz processor was ~ 80 minutes. Considerably faster processing times for model development and exploration can be achieved by reducing the number of MCMC simulations to achieve near convergence conditions.

2.3 Interannual Trend in Abundance

A meta-analytical approach was used to estimate a population trend for Rainbow Trout ≥250 mm over the 1999-2021 study period. The trend was estimated in a separate program that treated estimates of the log of annual abundance from the closed population model as data, but accounted for differences in uncertainty in the estimates. The model assumes that the log of abundance for the ≥250 mm size class follows a linear trend,

12) $$\hat{v}_y = \lambda_0 + \lambda \cdot (y - 1) + \epsilon_y$$

where $\hat{v}_y$ is the prediction of log-transformed abundance for each year y, λ_0 and λ are the intercept (log abundance in 1999 when y=1) and slope (rate of change/year) of the linear relationship, and ϵ_y are year-specific deviates representing process error. These deviates are drawn from a zero-centered normal distribution with an estimated standard deviation σ_e (i.e., $\epsilon_y \sim norm(0, \sigma\_e)$). λ is the parameter of interest as it represents the proportional change in the population per year. However, process error is also an important term, since it represents the true year-to-year variation in abundance around the trend.

The trend model is fit using a normal likelihood,

13) $$\boldsymbol{v_y} \sim norm(\hat{v}_y, \boldsymbol{sd}(\boldsymbol{v_y}))$$

where $\boldsymbol{v_y}$ and $\boldsymbol{sd(v_y)}$ are the mean and standard deviation of the posterior distribution of log abundance estimates from the closed population model. Years with greater uncertainty in annual estimates, because

they have only one-pass data or less informative mark-recapture data, will have higher values of $\mathbf{sd(\nu_y)}$ and contribute less to estimates of trend parameters (λ_0 and λ) compared to years with more precise estimates of abundance. Correct weighting of years in estimating the trend would also occur if the trend model was embedded in the abundance estimation model as in Cahill et al. (2018). However, the advantage of the two-stage approach used here is that the assumption of a linear trend in log abundance estimates will have no influence on the annual estimates from the closed population model.

The likelihood for the trend model (eqn. 13) provides an unbiased estimate of process error by removing the effects of observation error. That is, the model recognizes that some of the discrepancy between observed and predicted abundance in a given year is the result of uncertainty in the 'observed' abundance estimate. Without acknowledgement of observation error, the process error estimate from eqn. 12 would be inflated because it would include both true process error and observation error. Given that observation error in abundance estimates can be high, this is an important element to account for in the trend modelling.

Posterior distributions were estimated by taking every 15th sample from a total of 50,000 MCMC simulations after excluding the first 20,000 'burn in' samples for each of 3 chains (total posterior sample size of 2,000 per chain or 6,000 across chains). This sample size and sampling strategy was sufficient to achieve adequate model convergence that was evaluated using the Gelman Rubin convergence diagnostic (Rhat<1.05). Run-time on a computer with an Intel-i7 CPE @ 2.90 GHz processor was ~ 1 second.

2.4 Length-at-Age Modelling

2.4.1 Data and Comparison of Scale- and Otolith-Based Ages

The ageing data from the lower Bow River electrofishing program consists of samples collected during April, July, August, September, and October. Annual ages were determined from reads of scale and otoliths. For this analysis, I dropped the April samples because they would under-represent fish size at the end of the annual growing season and were rare (n=14). July and August samples may also under-represent size at the end of the annual growing season, but eliminating them would lead to a very large reduction in sample size (n=1600 for these months). After removing age samples without fork length (FL) measurements or that were collected in April, there were 4039 Rainbow Trout (RNTR) individuals that were aged based on scale reads, 109 individuals that were aged based on otolith reads, and 39 individuals that were aged based on both scale and otolith reads. A new field of individual fish age was created that used otolith-based ages if available and scale-based ages if otolith-based ages were not available. This resulted in 4148 age estimates for Rainbow Trout.

I examined the relationship between ages of Rainbow Trout individuals estimated from both scale and otolith reads. Assuming otolith-based ages are more accurate, the relationship can be used to evaluate if there is a potential bias in the scale-based ages. I also compared length frequency distributions of Rainbow Trout by age to examine the extent of overlap in fish size across annual ages to provide a non model-based approach of looking at the utility of fork length to predict age.

2.4.2 Estimating Proportion of Ages within Size Classes

I fit von Bertalanffy growth models to predict fork length as a function of age,

14) $$L_a = L_\infty \cdot (1 - e^{-K \cdot (a - a_0)})$$

where L_a is the fork length of a fish of age 'a' years, L_∞ is the asymptotic fork length (the average size of a fish at the terminal age), K is the Brody growth coefficient, and a_0 shifts the growth curve along the age axis to allow for apparent nonzero body length at age 0. As age determinations are generally taken from fall samples, a_0 represents the size of an age-0 fish in the fall. Separate von Bertalanffy (vB) growth models were fit to data for each year Rainbow Trout age estimates were available (1995 not included as n=1). The model was fit to the data in WinBUGS assuming error between predicted and observed fork lengths were normally distributed using the likelihood,

15) $$\boldsymbol{L_i} \sim norm(\hat{L}_i, \sigma^2_{tot})$$

where $\boldsymbol{L_i}$ is the observed length of individual 'i', $\hat{L}_i$ is the predict length from eqn. 14 given its age estimate, and σ^2_{tot} is the total variance estimate. The latter term is calculated from,

16) $$\sigma^2_{tot} = \sigma^2_{pro} + \boldsymbol{\sigma^2_{obs}}$$

where σ^2_{pro} is the estimated process variance in length-at-age resulting from variation in growth rates, and $\boldsymbol{\sigma^2_{obs}}$ is the observation variance in length measurements, which was assumed to be 9 mm. The observation variance was based on the standard deviation of error in length measurements of ± 3mm for Rainbow Trout measured in other studies (Korman et al. 2017, 2021). This variance estimation separates process and observation error, which is important to accurately estimate the process error. If observation error in length measurements is assumed to be zero when it is not, process error will overestimated. This in turn will lead to an exageration in the extent of variation in fish length within age classes which in turn influences estimates of the proportion of each age class within each length class. Note that σ^2_{pro} was assumed to be the same across years, though this constraint is easily relaxed.

Posterior distributions were estimated by taking every 10th sample from a total of 15,000 MCMC (Markov chain Monte Carlo) simulations after excluding the first 5,000 'burn in' samples for each of 3 chains (total posterior sample size of 1,000 per chain or 3,000 across chains). This sample size and sampling strategy was sufficient to achieve adequate model convergence that was evaluated using the Gelman Rubin

convergence diagnostic (Rhat<1.05). Run-time on a computer with an Intel-i7 CPE @ 2.90 GHz processor was ~ 5 minutes. Considerably faster processing times for model development and exploration can be achieved by reducing the number of MCMC simulations to achieve near convergence conditions.

Von Bertalanffy growth models were used to estimate the proportions of each age class within each of the six size classes for which Rainbow Trout abundance is estimated using the closed population model (<=200 mm, 200-249 mm, 250-299 mm, 300-399 mm, 400-499 mm, >=500 mm). Proportions in each age class were estimated using standard procedures for statistical catch-at-length models (Fournier et al. 1990). The predicted mean length at an age from the growth model (eqn. 14) for each year, and the process variance in length-at-age, was used to calculate the cumulative normal probabilities that a fish of age 'a' had fork lengths equal to the lower (e.g., 300 mm) and upper (e.g., 399 mm) boundaries of a length class. The difference between these probabilities represents the proportion of the age class within the size class. The procedure is repeated for all age classes within a size class, and then repeated across all size classes. Uncertainty in estimated age proportions in each size class was calculated by sampling the posterior distributions of vB parameters (eqn. 14) and the process error term (eqn. 15). The estimated proportions of age by size class were then used to translate abundance by length class determined from the closed population model to abundance by age class. This procedure accounts for uncertainty in age proportions by size class and the uncertainty in size class-specific abundance estimates.

I also developed an alternate way of estimating the proportion of ages classes in each size class without the assumption that length-at-age can be described by a continuous parametric function like the von Bertalanffy model. Here I assume that the number of observed ages within a size class is a multinomial-distributed random variable,

17) $$\boldsymbol{S_{isz,1:Nage}} \sim multinom(p_{isz,1:Nage}, \boldsymbol{NS_{isz}})$$

where **S** is the number of age estimates for each age (from age 1 to the maximum age Nage), p represents the estimated proportions of each age class in the age sample for the size class (*isz*), and **NS** is the total number of age estimates for the size class. This calculation is repeated for each size class for each year that age estimates are avaiable. The multinomial age proprotion model was implemented in WinBUGS and used uniformative Direchlet prior distributions for the proportion-at-age estimates. Posterior distributions were estimated by taking every sample from a total of 1,500 MCMC (Markov chain Monte Carlo) simulations after excluding the first 500 'burn in' samples for each of 3 chains (total posterior sample size of 1,000 per chain or 3,000 across chains).

2.4.3 Condition Factor

I calculated the condition factor for each Rainbow Trout in the Bow River electrofishing database by dividing its observed weight by the expected weight. The latter value was predicted based on the observed fork length and a length-weight relationship whose parameters were estimated from all Rainbow

Trout length-weight observations ($W=e^{-9.836+2.748 \cdot \log(L)}$, n=9,191). Thus, fish with condition factors (CFs) > 1 are heavier than expected given their length and are considered to have better than average condition, while those with CF<1 are lighter than expected and considered to have poorer than average condition. As condition factor can vary among size classes, statistics on condition factor were summarized for 0-299 mm, 300-449 mm, and ≥450 mm size classes.

3.0 Results

3.1 Capture Probability from Closed Population Model

The model estimated that capture probability generally increased with fish size (Fig. 2 and Fig. 3, top-left panel). Capture probability on pass 2 was slightly higher than on pass 1 and declined from passes 2 through 4 (Fig. 3, top-right panel). Capture probability on pass 5 was highly uncertain. The magnitude of pass effects was modest, with maximum expected effects of ~ ± 0.2 on the logit scale. There was a generally increasing trend in capture probability across years (Fig. 3, lower-right panel). Year effects were substantive, with a maximum difference across years (2001 vs. 2021) of 1.25. Higher uncertainty in β_y estimates in 2017, 2019, and 2020 occurred because there was no mark-recapture sampling (Table 1). The β_y estimate in 2021 had the highest precision because mark-recapture data was more informative given more recaptures.

Site effects on capture probability (β_s) were generally very small (medians close to zero) and highly uncertain (Fig. 4). Effects for sites that were repeatedly sampled across years (e.g., sites 304.5, 305.5, 306.5, 307.5) were more precisely estimated than from sites sampled once or twice across years (Fig. 4a). β_s estimates for one-pass sites are simply random draws from the hyper-distribution, and were therefore centered on zero with larger uncertainty (determined by σ_s) compared to estimates from the mark-recapture sites that were repeatedly sampled across years (Fig. 4b).

An example of capture probability estimates for the fourth size class is presented in Figure 5 to demonstrate the effects of year, pass, and site effects in untransformed (i.e., 0-1) space. Here we see that the effect of pass is relatively minor compared to the effect of year. The position of the site-specific points (blue open points) relative to the range of the year-pass estimates (black points and error bars) demonstrates how site and especially process error allow flexibility in capture probability estimates to best fit the data (e.g., capture probability at one site in 2021 on pass 4 was unusually high). Process error was almost 2-fold higher and considerably more precise than site error (Table 4) indicating the former was the dominant cause for the variation around year-pass predictions of capture probability (Fig. 5).

I fit a model that accounted for potential differences in capture probability between fish that were previously captured (eqn. 10) and those that were not previously captured (eqn. 1). The previous capture effect (γ in eqn. 10) was not estimable using an uninformative prior (sd=1000). This occurred because there was insufficient information about the capture probability of unmarked fish (not previously caught) because of the limited depletion of the unmarked population across passes. I therefore used a more informative prior on γ with a standard deviation of 0.31. The mean of the posterior distribution for the previous capture effect (γ) was positive indicating a potential trap-happy effect (0.42 with 95% credible intervals of -0.03 – 0.85, Fig. 6). For the most common size class (400-500 mm, Fig. 1) the mean γ estimate resulted in a capture probability for unmarked fish of 0.029, compared to a capture probability for marked fish of 0.044. In other words, previously captured fish were ~ 1.4-fold more vulnerable to capture than unmarked fish. In spite of the more informative prior, the coefficient of variation (CV=standard deviation/mean) for γ was 0.53, and the 95% credible intervals were very wide and even spanned zero. The prior on γ had an important influence on the posterior estimates given extensive overlap between the two distributions (Fig. 6). The prior limited the upper range of γ estimates. Taken together, these results indicate that γ is poorly determined from the data, though there is evidence for a trap-happy effect due to previous capture. This implies that the capture probability of unmarked fish, which form the vast majority of the catch, is lower than for marked fish. As will be shown below, including a previous capture effect leads to an increase in abundance estimates relative to models which do not account for this effect.

Estimates of the probability that a recaptured fish was caught in a site other than the one it was originally marked in (θ_y) were generally well determined by the data (Fig. 7, Table 3). The median of the mean of the θ hyper-distribution (eqn. 5) was 0.16. There was considerable variation in the movement-related mark loss rate across years, with a peak of 0.4 (logit space) in 2001 and a low of 0.04 in 2012. There was generally a strong correspondence between independent estimates of θ_y (blue points in Fig. 7, Table 3) and estimates from the model (which in logit space were assumed to arise from a common normal distribution). As expected from this hierarchical structure, the model shrunk independent θ_y estimates that were further from the mean towards the mean of the hyper-distribution, but only when sample size was low (e.g., 2000, 2005, 2012). In contrast, if an independent estimate was far from the mean but sample size was large (e.g., 2001) there was very limited shrinkage towards the mean. In this case there was sufficient data on the out-of-site movement rate to resist statistical shrinkage. Shrinkage due to the effects of the hierarchical structure on θ_y estimates will be greater for species other than Rainbow Trout where sample size is smaller (Table 3).

3.2 Abundance

Size class- and site-specific estimates of abundance at mark-recapture sites across the study period were variable, and estimates were sometimes highly uncertain owing to limited numbers of recaptures (Fig. 8). High uncertainty in site-specific abundance estimates was particularly evident in 2000 and 2001 due to low numbers of recaptures. In contrast, more recent years, especially 2021, provided precise site-specific abundance estimates for almost all size classes due to a higher number of recaptures. In most years, the variation in Rainbow Trout density (fish/km) across the four consistently sampled mark-recaptures sites was very small, with CVs of across-site densities ranging from 0.01 (2021) to 0.10 (2018). Greater variation in fish densities across sites was observed in years when more mark-recapture sites, or one-pass sites, were included (Table 1, 2001, 2013, 2018-2020), with CVs ranging from 0.11 (2018) to 0.38 (2001).

Annual abundance estimates based on data from only mark-recapture sites indicated higher abundances in 2000, 2001, and 2007 (Fig. 9). In most years the precision of the size-aggregated abundance estimates was reasonable (e.g., 95% credible interval in 2008 of ~600-1300 fish/km, average CVs for annual estimates ~0.30). However, there was substantial overlap in credible intervals of abundance for many years. Precision of size-aggregated abundance was highest in 2021 (CV= 0.11) because precision in site-specific abundances was highest (Fig. 8). Among size classes, abundance was generally highest in the 400-500 mm size class.

Site-specific abundance estimates at one-pass sites were more uncertain than at mark-recapture sites owing to greater uncertainty in capture probabilities (Fig. 10). For example, the average CV for size-aggregated abundance estimates across the four mark-recapture sites sampled in 2018 was 0.26. In contrast, the average CV in size-aggregated abundance estimates across the 12 one-pass sites sampled in 2018 was 0.66. As a result of this difference, annual abundance estimates based on mark-recapture (average CV across years of 0.22) were more precise compared to those based on one-pass sites (average CV across years = 0.56, Fig. 11) even though there were considerably more one-pass sites than mark-recapture sites sampled within years. Comparisons in 2001, when both mark-recapture and one-pass sites were sampled and when mean abundances were similar across site types, show the considerably higher uncertainty in annual abundance estimates based on data from one-pass sites. A key advantage of the model is that it integrates estimates of abundance from mark-recapture and one-pass sites, providing a better representation of the population (Fig. 12a). The lower precision in years with only one-pass data (2017, 2019, 2020) was evident.

The average of size-aggregated abundance estimates across years was 883 fish/km (Fig. 12a). The average based on the model that included a previous capture effect on capture probability (Fig. 12b) was

1206 fish/km, a 1.4-fold increase in abundance. Abundance was higher based on the latter model because the capture probability for unmarked fish, which make up the vast majority of the catch, was lower, because the previous capture effect, applied to marked fish, was positive (eqn. 10). As previously shown, the estimate of the previous capture effect was influenced by an informative prior distribution (Fig. 6). Thus, the abundance estimates from the model that do not include a previous capture effect (eqn. 1, Fig. 12 a) should be considered more reliable at this time. However, the model which includes a previous capture effect suggests that the true estimates of abundance may be higher than those determined from the base model by a minimum of ~40%.

Estimates of uncertainty in abundance estimates at mark-recapture and one-pass sites can be used to calculate their combined effect on the uncertainty in annual estimates of abundance to in turn guide future decisions on sampling effort. All else being equal, the precision of annual abundance estimates should increase with the number of sites sampled owing to the law of large numbers. This can be demonstrated using two of Goodman's variance formulas (Goodman 1962, https://en.wikipedia.org/wiki/Variance). The first is that that the variance of a sum of uncorrelated random variables is the sum of their variances. In this application,

18a) $$V_{tot} = V_{s=1} + V_{s=2} + \cdots$$

where V_{tot} is the total variance of the annual population estimate (for a size class) and Vs=1… are the variances of the site site-specific abundance estimates. As the annual population estimates are standardized to 1 km of stream length (Vkm_{tot}), I used Goodman's second formula, which calculates that the variance of the product of a constant (a) and a variance (Var(a·X) is equal to the product of the square of the constant and the variance ($Var(a \cdot X)=a^2 \cdot Var(X)$). In this application the constant is 1000 divided by the sum of site lengths surveyed in a year, thus the variance is calculated from,

15b) $$Vkm_{tot} = \frac{1000}{L_s^2} \cdot V_{tot}$$

where L is the sum of site lengths in meters.

To demonstrate the effect of site-specific uncertainty on the annual population estimates, I use a scenario with equal fish densities across sites and a CV of fish density estimates of 0.26 (the across-site average CV in site-specific abundance estimates (summed across size classes) from mark-recapture sites in 2018). The CV of the annual abundance estimate declines from 0.26 with one site sampled to an asymptotic level of ~ CV=0.05 if 16 mark-recapture sites are sampled (Fig. 13). In 2018, only four sites were sampled with the remaining sampled by one-pass of effort, where the model-based average of site-specific CV's (in 2018) was 0.66 (higher uncertainty as capture probability not determined at one pass sites). Including just one one-pass site in the calculation of the annual estimate previously based on four mark-recapture sites results in a decrease in precision of the annual estimate (Fig. 13, CV increases from ~0.13 to 0.17). As the number of one-pass sites contributing to the annual estimate increases, the CV

declines (again due law of large numbers), but relatively slowly because of the higher uncertainty in population estimates from the one-pass sites. The CV of the annual estimate based on four mark-recapture sites and 12 one-pass sites (the effort in 2018, Table 1) is just a bit higher than the CV of the annual estimate based on just four mark-recapture sites. This result does not imply it is not worth sampling one-pass sites. Although the precision of the annual estimates degrades slightly, the inference about the abundance of Rainbow Trout in the Bow River is much stronger because a much higher proportion of the population is sampled compared to the 4-mark-recapture site case.

3.3 Interannual Abundance Trend

There was a weak negative trend in the abundance of Rainbow Trout ≥ 250 mm over the study period (median λ=-0.031/year (3.1%) with 95% credible intervals of -0.061 - -0.001, Fig. 14). The median rate of decline predicts the population in 2026 (5 years from 2021) and 2031 (10 years from 2021) would be 86% and 73% of its abundance in 2021. The 95% credible interval for the trend line (dark grey band in Fig. 14) is determined based only on the uncertainty in the trend model terms (λ_0 and λin eqn. 12. The wider 95% credible interval around the trend line (light grey band) includes both the uncertainty in the trend line and effects of process error (σ_e = 0.32 with 95% credible intervals 0.12 – 0.58). This interval represents the potential range of annual estimates given the trend and the extensive year-to-year variation in abundance around the trend.

3.4 Length-at-age Modelling

Fry from spring-spawning Rainbow Trout in the Bow River and its tributaries will emerge from redds in late May to early July (determined based on spawning period of early may to mid June reported by Rhodes 2005). This late emergence results in a very short first growing season for age-0 fish, which can make the first winter growth check difficult to detect. It is possible that the first winter check is more difficult to detect in a scale compared to an otolith, and thus we might expect otolith-based ages to be older compared to scale-based ages. Fortunately, there was generally good correspondance in the age estimates for the 39 Rainbow Trout that were aged using both methods (n=8 in 2012, n=31 in 2013, Fig. 15). There was tendancy for otolith-determined ages to be one or two years older than scale-based age estimates for scale ages 1, 3, and 4 years. However, otolith-based ages were not higher than scale-based ages for ages 2, 5, and 6, perhaps indicating that there is no bias in scale-based ages.

When data were aggregated across collection years, median size within ages increased with age (Fig. 16). However, there was considerable overlap in size distributions across ages, especially for fish age 4

years and older. For understanding factors driving variation in abundance over years, the most important age classes to separate are ages 1 and 2 years, since the abundance of age 1 fish can be used as a measure of recruitment to the surveyed Rainbow Trout population. Figure 17a compares size distributions for fish aged 1 and 2 years, by collection year. In most years, age 1 and 2 year fish are generally less than and greater than 250 mm, respectively. However, due to variation in growth, the size to separate these ages can vary across years, and can be as high as 300 mm (2003) and as low as 200 mm (2013). In addition, the extent of overlap in size between age 1 and 2 year fish varied considerably across years, from a low of 7% (2003, 1999 excluded due to low sample size) to a high of 77% (2012). The extent of overlap among adjacent ages increased with age (Fig.'s 17b and 17c). This result is not surprising as variation in growth rates among individuals leads to increasing overlap in size distributions between ages as age increases.

Von Bertalanffy (vB) length-at-age models fit the data well (Fig. 18a). There was considerable variation in median estimates of the Brody growth coefficient (K) and the asymptotic size (L_∞) across collection years. Length-at-age was substantively lower in 2012 and 2013 compared to earlier years (Fig. 18b). Von Bertalanffy models were used to predict the proportion of each age class with a size class, for all size classes and collection years (Fig. 19). In general, most age 1 fish were < 250 mm. However, there could be a substantive proportion of age 1 fish in the 250-300 mm size class in some years (e.g., 2003), and substantive proportions of fish in the 200-250 mm size class that were age 2 (2012, 2013). Thus, it is not advisable to use a fixed set of size classes to index recruitment (age 1 abundance) across years. The age proportion results also demonstrate that larger size classes (300-400 mm and greater) consist of multiple age classes. As growth decreases with increases in size (Fig 18), the larger the size class, the greater the number of age classes it represents. Owing to variation in growth rates over years, the size-age relationships were variable among years (Fig. 18b), leading to variability in the proportion of age classes within a size class among years (Fig. 20). Thus, a sufficient sample of ages are needed in each sampling year to reliably determine age proportions.

Uncertainty in vB-based estimates of age proportions with size classes was high in years when the sample size of age estimates was low (Fig. 20a, 1999) compared to when it was high (Fig. 20b, 2013). In some cases (e.g., 1999), the estimated age proportions were well determined for larger size classes (e.g., 400-500 mm) but poorly determined for smaller ones (e.g., 250-300 mm) owing to a very limited number of age determinations for smaller/younger fish (Fig. 18a). The reliability of multinomially-based age proportions within size classes was much lower compared to the reliability of age proportions estimated by vB models (Fig. 21). This occurs because the multinomial model does not assume an underlying growth relationship and therefore does not borrow information about age-length across size classes as the vB model does. The multinomial approach also assumes that the available ages are from a random sample of the catch. Owing to these differences, the multinomial model was very sensitive to the sample sizes of age determinations within each size class, sometimes providing non-sensical results. For

example, only two fish >500 mm were aged in 2013 even though the total sample size for that year was 220 fish (Fig. 21b). One fish was 4 years old and the other was 5 years old, so the model estimated that the proportions of these age classes in the > 500 mm size class were both 0.5 but with high uncertainty,. Owing to the limited sample size the model assigned near zero probability for fish being older than age 5 in this size classes, which was not consistent with the length-age relationship in 2013 (Fig. 18) and its estimates of age proportions for this size class (Fig. 20b).

Estimated age proportions within each size class was used to translate abundance by size class into abundance by age class. These calculations are possible for years when both age and abundance estimates are available (Fig. 22). Patterns in 1999, 2012, 2013, and 2021, when abundance of age 1 year fish were similar to abundances of older fish, indicate limited recruitment in those years (i.e., relatively few younger fish entering the population). Other years (e.g., 2000, 2001, 2003, 2011) had substantially higher proportions of age 1 fish indicating higher levels of recruitment. Other statistics from abundance-by-age estimates are easily calculated, such as the implied survival rate of older fish based on the rate of decline in abundance across older ages (i.e., catch-curve type analyses).

Fork length of Rainbow Trout was a good predictor of weight (r^2 =0.98, p-value < 0.001, Fig. 23). Observations above and below the best-fit length-weight regression line represent fish with above and below average condition factor, respectively. However, the scatter is also driven by error in length and weight observations. Condition factor in 2012 and most later years was generally lower than earlier years, and the magnitude of this difference was greatest for Rainbow Trout > 450 mm (Fig. 24). Larger fish have greater energetic requirements, and thus show the greatest decline in condition when prey intake is reduced due to either reductions in prey supply or increased competition for prey, or other negative effects such as elevated water temperatures.

The condition factor calculations describe relative variation in weight within the Bow River Rainbow Trout population only, and do not describe the condition of these fish relative to other populations. I therefore plotted the Bow River length-weight relationship relative to one representing lotic populations of Rainbow Trout summarized in Blackwell et al. (2000), and a population of Rainbow Trout in the Colorado River downstream of Glen Canyon Dam (Korman et al. 2017, Fig. 25). The length-weight relationships from the Bow River and Blackwell et al. populations were virtually identical. Rainbow Trout in the Colorado River were skinnier compared to the Bow River population.

4.0 Conclusions and Recommendations

4.1 Abundance Modelling

The capture probability model explicitly accounts for the effects of fish size, year, site, and pass, and therefore provides insights into key factors that determine the conversion of catch into abundance estimates. Fish size had the greatest effect on capture probability, ranging from ~ 1% for the smallest size class (≤ 200 mm) to ~ 9% for the largest (≥ 500 mm), a 9-fold difference. Year was also an important determinant of capture probability. The capture probability for the most dominant size class (400-500 mm) ranged from a low of ~4% in 2001 to a high of 13% in 2021, a 3-fold difference. There was limited or no overlap in 95% credible intervals of capture probability between early (1999-2003) and most later years (2011-2013, 2020, 2021). This extensive year-to-year variation has important implications with respect to abundance trends. For example, if catch in 2001 and 2021 had been the same, the model would estimate that abundance in 2021 would have been ~ 1/3rd of the abundance in 2001 (because capture probability in 2021 was ~3-fold higher). Year effects on capture probability were generally well-determined in years when mark-recapture experiments were implemented. Uncertainty in year effects was considerably greater in years when only one-pass sampling was done, highlighting the need to conduct mark-recapture sampling in all future years that are monitored.

The effect of sampling site on capture probability was poorly determined because the number of recaptures within sites was generally low. Logically, site-specific effects were slightly better-determined for the four mark-recaptures sites that have been consistently sampled in most years. There was weak evidence that capture probability was slightly less at sites 304.5 and 305.5 compared to 306.5 and 307.5, but differences were modest. For example, capture probability for the dominant 400-500 mm size class was approximately 6% at the first two sites and 8% at the second two. Based on the extensive overlap in credible intervals, these potentially small differences in capture probabilities among sites are not statistically distinguishable. Capture probability on pass 2 was slightly higher than on pass 1, and decreased between passes 2 and 4. However, differences were modest. For example, the capture probability for the 400-500 mm size class on pass 1 was ~7%, 9% on pass 2, and then declined to 6% by pass 4. I speculate that the initial increase in capture probability between passes 1 and 2 could be the result of boat operators learning to fish the site more thoroughly after completing the first pass, with declines on later passes resulting from the disturbance effect of electrofishing over consecutive days. On average, 16% of Rainbow Trout marked in a site were estimated to move to other sites between release and recapture events within a year. The model must account for this mark loss rate because it estimates abundance at the site level. Mark loss was highly variable across years (4-40%) and may have been

higher in 2001 (40%) due to a longer period between release and recapture events or because only one bank was sampled.

The estimate of the long-term trend in abundance of Rainbow Trout in the Bow River indicates the population is declining at a rate of ~3%/yr. This rate of decline is half of the mean estimate from Cahill et al. (2018) for the 2003-2013 period of ~ 6%. The difference in estimates of the trend between studies is likely due to a combination of differences in model structure, input data, and the period of evaluation (1999-2021 for the trend presented here, vs. 2003-2013 used in Cahill et al. 2018). The analysis presented here indicates there is substantive year-to-year variation in abundance around the declining trend. Over longer time periods of time, the low annual rate of decline can lead to substantive reductions in expected abundance. For example, the annual rate predicts that abundance in 2031 will be ~ 73% of the trend-based prediction in 2021. However, given the uncertainty in the trend, and more importantly, the extensive year-to-year variation around it, predictions of future abundance should be considered highly uncertain.

The trend in the abundance of size classes over years is not consistent with the expectation that the survival rate of fish after the age of recruitment (i.e., ~>200 or 250 mm) is stable. Trends for 2017-2021 provide an illustrative example. The higher abundance of ≤200 mm Rainbow Trout in 2018 and 2019 should have been followed by higher abundance in the 200-250 mm and 250-300 mm size classes in 2019 and 2020, respectively. This did not occur. Reduced abundance for ≤200 mm trout in 2020 was followed by higher abundances of larger size classes in 2021. There are two possible interpretations for these patterns. First, the patterns may largely be driven by observation error (uncertainty in the year- and size class-specific abundances). The other possibility is that the trends based on the annual size-specific abundances are correct, but the limited length of the Bow River that is sampled each year does not provide a good representation of the abundance of all size classes in the population. For example, larger fish that originated from locations other than the sampled area could settle in the sampled area following migrations to tributaries to spawn. Additional analyses could help partially resolve this uncertainty. The electrofishing-based information on movement of tagged fish between sites across years (n=80 for Rainbow Trout and n=114 for all species) could be interrogated to evaluate the potential extent of movement and site fidelity within the study area. The extent of larger movements could be assessed using data from radio telemetry surveys (e.g., Rhodes 2005). In addition, length-at-age and abundance modelling could be combined in a statistical catch-at-age model to jointly estimate annual recruitment, survival, and growth, providing a more integrated analysis of the data. This would provide a more rigorous assessment of the extent of variation in recruitment and survival rates (by size class) across years relative to eyeball-type assessments such as the initial interpretation provided here. However, this model may be difficult to apply given missing years in the time series of abundance estimates.

The closed population model presented here has a number of advantages compared to previous efforts. First, the model integrates data from both mark-recapture and one-pass sites, providing more spatially

representative estimates of abundance for 5 of the 15 years of available data between 1999 and 2021. The model allows a comparison of variance in abundance estimates at mark-recapture and one-pass sites, which can be used to better distribute future sampling effort between these two types. Second, the model estimates abundance at the site level. Thus, it does not assume that capture probability across sites is homogenous as do earlier assessments, which could lead to substantive bias in annual abundance estimates if capture probability and abundance vary across sites. The model allows for potential exploration of habitat or other site-specific effects on abundance. Third, the model structure is simpler, easier to understand and computationally efficient compared to the data augmentation approach used in Cahill et al. (2018), which required long run times, informative priors, and substantial structural assumptions. Fourth, the structure of the capture probability model, which includes fixed effects of fish size and pass, and random effects of year and site, provides insights into the factors that affect the magnitude and precision of capture probability estimates, which has direct implications for future monitoring efforts. Finally, the model runs relatively quickly, reaching convergence in ~ 80 minutes (for six size classes, considerably less for fewer size classes), with much quicker execution times (to reach near convergence conditions) for model development and exploration of alternate structures. The model presented here uses the traditional and commonly-used MCMC methodology available in BUGS, JAGS, and other Bayesian software packages. The combination of the simpler model structure and faster run times reduces the probability of coding errors and allows analysts with less background in mark-recapture and Bayesian models to better understand, use, and modify the model in the future.

The precision of annual abundance estimates of Rainbow Trout in years with mark-recapture sampling has been much higher in recent years. The interannual trend in capture probabilities suggest that the quality of electrofishing effort has improved, likely because boat operators and netters have more experience. The resulting higher and more precisely-defined capture probabilities have led to a substantive increase in the precision of annual abundance estimates (e.g., 2021). The precision of annual abundance estimates from early years (1999, 2000, 2001 with CV's 0.28-0.31) were much lower compared to more recent years (e.g., 2021, CV=0.11). The mark-recapture data from 2001 highlights the potential negative effect of less experienced crews. Here 46 and 197 mark-recapture and one-pass sites were sampled, respectively, compared to only four mark-recapture sites sampled in 2021. Owing to the law of large numbers, all else being equal, the precision of the annual abundance estimate in 2001 should have been much higher than in other years. However, precision of site-specific abundance estimates in 2001 (CV=0.29) was substantially lower because capture probability was lower causing both a lower overall catch and lower number of recaptures. Other factors could have contributed to the low precision of abundance estimates in 2001. Out-of-site movement in 2001 was also considerably higher than in other years, perhaps because of the longer intervals between passes (average of 11.6 days across 71 multi-pass sites) compared to other years when mark-recapture was done (1 day), or because mark-recapture sites in 2001 only included one bank.

Precision of annual abundance estimates will be higher if based only on mark-recapture sites then based on a combination of sites sampled by mark-recapture and one-pass methods. This occurs because the precision of abundance estimates at one-pass sites is ~2.5-fold lower compared to mark-recapture sites. However, owing to the law of large numbers, including ~ 12 one-pass sites in the annual estimate of abundance did improve the precision to a level that was approximately equivalent to what would occur if only four mark-recapture sites were used to estimate annual abundance. The approach of using both mark-recapture and one-pass sites to calculate annual abundance estimates provides a stronger inference about the abundance of trout in the Bow River since a much larger proportion of the total stream is included in the estimate due to the addition of one-pass sites. The evaluation of combined use of mark-recapture and one-pass sites on the precision of annual estimates presented here did not consider effects of variation in densities across sites, and therefore undersells the benefits of sampling more sites via one-pass. Direct estimation of across-site variation in fish density across sites in the closed model would be required to parameterize a simulation model to better quantify the benefits associated with different combinations of mark-recapture and one-pass sites (e.g., Korman et al. 2016). However, the analysis of the data suggests the current approach on the Bow River of sampling 4 mark-recapture sites in the first week, and ~ 12 one-pass sites in the second, is sound.

There were differences between the estimates of abundance of Rainbow Trout in the Bow River presented here and those from previous efforts. The estimates of annual abundance were higher than those from Cahill et al. (2018). For example, median estimates of abundance in 2003, 2005, 2007 and 2008 from Cahill et al. were ~ 400 fish (≥250 mm) /km. In contrast, the estimates of median abundance over these years in this analysis ranged from ~500-900 fish (≥250 mm)/km. Without an examination of the code and data used in Cahill et al., the causes for these differences are uncertain. Henderson (2013) estimated that rainbow trout abundance in two reaches in the Bow River (all size classes) was 150 and 893 fish/km, with an average of 469 fish/km. These estimates were generated using program MARK, an established method for estimating abundance from mark-recapture data. The estimate of abundance across all size classes in 2013 presented here was ~ 600 fish/km, slightly higher than the across-reach average of 469 fish/km from Henderson (2013), but comfortably within the range of the two site-specific estimates. Cahill et al.'s estimate for Rainbow Trout ≥250 mm in 2013 was ~ 60 fish/km, ~ 5-fold lower than the across-reach average estimate (≥300 mm) of 315 fish/km from Henderson (2013), and ~8-fold lower than the estimate of 520 fish (≥250 mm)/km presented here. However, Cahill et al.'s (2018) abundance estimate for 2013 was based on only one site located at the upstream end of the survey area. Henderson reported that capture probability for rainbow trout ≥300 mm was 0.17-0.18 across the two reaches they surveyed. Based on the raw data used in this analysis, the capture probability for this size class using data from all four mark-recapture sites was 0.08-0.11. Again, without examination of the data and models used in Henderson (2013), I was unable to explain why the reported capture probability was higher than the calculated values from the raw data that was used.

The overall capture probability for Rainbow Trout in the Bow River ranged from about 1% for the smallest size class (≤ 200 mm) to ~9% for the largest size class (>500 mm), and was 7% for the dominant size class (400-500 mm). These estimates are broadly comparable to those for Rainbow Trout in the Colorado River in Glen Canyon. Korman and Yard (2017) used mark-recapture and nighttime boat electrofishing to estimate capture probability for trout at large for one day (within-trip) and for 2-3 months (across-trip). Based on a model similar to Korman and Yard and using all data available to date (through November 2022), within-trip capture probabilities in Glen Canyon ranged from ~12% for trout 75-124 mm to 5% for trout ≥275 mm. Across-trip capture probabilities for trout were ~13% to 2% across these same size classes. There are three interesting differences between the capture probability estimates from the Bow and Colorado rivers.

First, the Bow River estimates are surprisingly high given that daytime boat electrofishing has been shown to have considerably lower capture probability than nighttime sampling (Sanders 1991, Pierce et al. 2011). Second, the size-specific trends in capture probabilities among the two systems are completely opposite, with capture probability in the Bow River increasing with fish size but declining with fish size in the Colorado River. Third, capture probabilities for trout > 225 mm in the Colorado River are considerably higher for those at large for one day (~5%) compared to those at large for 2-3 months (~2%). This difference is interpreted as a trap-happy effect that is only present in fish at large for one day due to immediate effects of capture, handling, and release in a concentrated area in the middle of each site. These effects on capture probability are hypothesized to dissipate over the two to three-month period between survey trips.

There is weak evidence in the Bow River data that previously captured fish (at large for 1-4 days) have a higher capture probability than unmarked fish that have not been previously caught in the same survey year. Capture probabilities in 2001, when time at large between passes (~ 11 days) was considerably longer than in other years (1 day) also supports the possibility of a trap-happy effect due to the short interval between passes.

It is possible that this potential trap-happy effect for Bow River Rainbow Trout is the result of the same capture-handling-release impact hypothesized to be affecting capture probabilities for trout at large for only 1 day in the Colorado River. This provides further support that capture probability for unmarked fish in the Bow River is lower than for marked fish, and thus that abundance is underestimated in the base model presented here (which doesn't account for this effect). Additional modelling work to estimate a previous capture effect is warranted.

The capture probability and abundance results from the model lead to the following recommendations for future sampling:

1) Mark-recapture should be continued at the standard four sampling sites in each year sampling is conducted;

2) Given the limited number of recaptures at each site, all target species (Rainbow Trout, Brown Trout, Mountain Whitefish) above the minimum taggable size should be tagged;

3) One-pass sampling provides a meaningful contribution to abundance estimates, but only if conducted in years when some sites are sampled by mark-recapture; and

4) Boat operator and crew experience may be having important effects on capture probability and hence the precision of abundance estimates. Thus, proper training and careful blending of experienced and new crew is warranted.

Potential modifications to the model and additional analyses to improve inferences about capture probability and abundance include:

1) Further evaluation of a previous capture effect on capture probability. This effect may be estimable with a less informative prior than used here, especially if the number of size classes is reduced or other justifiable constraints are implemented. Year-specific previous capture probability effects are potentially estimable using a hierarchical structure similar to the one used for out-of-site movement-related mark loss;

2) The effects of the Poisson and binomial likelihoods (used to fit the model to unmarked catch data) on estimates of model uncertainty should be investigated. Applying the binomial likelihood to unmarked catch data would require adjustments to the model's initial conditions as well as to the prior distributions for site-specific abundance;

3) Further evaluation of the two methods to expand catches at one-pass sites (i.e., with or without sampling error, eqn. 11a vs 11b) is needed. It is unclear whether the model with sampling error would converge if slightly more informative priors were used, or if random draws from the process error distributions were constrained.

4) Almost half of the mark-recapture data used in this analysis was generated in 2001, a year with low capture probability and an unusually high rate of movement of marked fish to other sites. It is possible there are other problems with the 2001 data that are not accounted for in the model. Rerunning the model without the 2001 data would be useful to evaluate this potential issue.

5) The model should be applied to data on Brown Trout and Mountain Whitefish. Owing to sparser mark-recapture data for these species, more informative priors, reductions in the number of size classes that are modelled, or the use of a parametric function to predict size variation in capture probability, may be required;

6) Simulation modelling can be used to evaluate the effects of different levels of sampling intensity (number of mark-recapture and one-pass sites) on the precision of population estimates. A critical component of this analysis will be estimation of across-site variation in fish density.

It is likely that the majority of these analysis and model changes (focused on Rainbow Trout, i.e., 1-4) will not result in substantive changes to the abundance estimates reported here, or at least to the interannual trend in abundance. Modifications that produce a reliable model that includes a previous capture effect (1) could lead to substantially higher estimates of abundance but would not impact the trend in abundance unless year-specific previous capture effects were estimated.

4.2 Length-at-Age Modelling

There was reasonable agreement between otolith- and scale-based age estimates for Bow River Rainbow Trout, however the sample size of individuals aged by both methods was small. Von Bertalanffy growth models fit the length-at-age data well and predicted asymptotic sizes ranging from ~520 – 640 mm across years. Length-at-age was substantively lower in 2012 and 2013, at intermediate levels in 2017 and 2021, and higher in other years (1999-2001, 2003, 2005, 2011, 2014). Although there is substantive overlap in size ranges among adjacent ages (especially for older fish), von Bertalanffy models were effectively used to convert abundance by size class into abundance by age class. The resulting multi-year time series of abundance by age class can be used to provide insights about population dynamics. For example, variation in the abundance of age 1 trout over years describes the extent of variation in the number of new recruits entering the population. Changes in the slope in the decline in abundance across ages within years can be used to evaluate whether mortality rates of older age fish are changing to assess effects of fishing regulations. Larger Bow River Rainbow Trout showed a modest decline in condition factor between 1999 and 2021.

Ageing data from trout on the Bow River was useful both for assessing variation in growth rates over time, and for translating size-based abundance estimates into age-based ones. Given evidence that growth rates and hence length-at-age has varied across years, continuation of age sampling is warranted. Sample sizes in 2014 and later years, when age determinations were largely made using otoliths, has been small. Small sample size results in greater uncertainty in von Bertalanffy models, and hence greater uncertainty in translation of size- to age-based abundance. Thus, increasing the annual sample size of scale-based age estimates is recommended. A size-stratified age sampling design would ensure there are sufficient samples across the full range of size classes, which in turn will lead to greater certainty in estimated length-at-age relationships. Obtaining a minimum of 20 age estimates for each of the size classes used in the abundance modelling requires a final sample size of 120 age determinations per year, which might require a sample of up to 150 scales given potential scale regeneration in some samples. Given the small sample size of individuals aged by both otolith and scales, a small size-stratified sample of individual fish aged by both methods each year is recommended. These data will contribute to a more robust determination of the accuracy of scale-based age estimates than could be presented here and can also be used to verify that annual age estimates continue to be accurate.

Potential extensions of the age-based modelling include:

1) Development of covariate models to predict changes in von Bertalanffy growth parameters to determine factors driving variation in growth rates over time;

2) Development of a simple population dynamics model that estimates annual recruitments and age 2+ year survival rates by fitting to the multi-year age-based abundance estimates. Note that recruitment and survival rates will be difficult or impossible to estimate in some years because of the multi-year gaps in electrofishing sampling.

5.0 References

Blackwell, B.G., Brown, M.L., and D. W. Willis. 2000. Relative weight (Wr) status and current use in fisheries assessment and management. Reviews in Fisheries Science 8: 1-44.

Cahill, C.L., Morgensen, S., Wilson, K.L., Cantin, R., Sinnatamby, N., Paul, A.J., Christensen, P., Reilly, J.R., Winkle, L., Farineau, A., and J.R. Post. 2018. Multiple challenges confront a higher-effort inland recreational fishery in decline. Can. J. Fish. Aquat. Sci. 75 (9). https://doi.org/10.1139/cjfas-2018-0086

Fournier, D.A., Hampton, J., and J.R. Sibert. 1998. MULTIFAN-CL: a length-based, age-structured model for fisheries stock assessment, with application to the South Pacific albacore, *Thunnus alalunga*. Can. J. Fish. Aquat. Sci. 55: 2105-2116.

Goodman, L.A. 1962. The variance of the product of K random variables. J. Am. Stat. Assoc. 57: 54-60.

Henderson, S. 2013. Bow River Sportfish Population Monitoring 2013. Draft report prepared by the Fisheries Management, Alberta Environment and Sustainable Resource Development. 39 pp.

Hilborn, R., and M. Mangel. 1997. The ecological detective, confronting models with data. Princeton University Press, Princeton, NJ. 315 pp.

Korman, J., M.D. Yard, Dzul, M.C., Yackulic, C.B., Dodrill, M.J., Deemer, B.R., and T.A. Kennedy. 2021. Changes in prey, turbidity, and competition reduce somatic growth and cause the collapse of a fish population. Ecol. Monog. 91(1).

Korman, J., M.D. Yard, and T.A. Kennedy. 2017. Trends in rainbow trout recruitment, abundance, survival, and growth during a boom-and-bust cycle in a tailwater fishery. Trans. Am. Fish. Soc. 146:1043-1057.

Korman, J., and M. D. Yard. 2017. Effects of environmental covariates and density on the catchability of fish populations and interpretation of catch per unit effort trends. Fisher. Res. 189: 18-34.

Korman, J., Schick, J., and B. Mossop. 2016. Estimating riverwide abundance of juvenile fish populations. How much sampling is enough? Nor. Am. J. Fish. Manage. 36:213-229.

Millar, R.B., and M.J. Anderson. 2004. Remedies for pseudoreplication. Fisheries Research 70:387-407.

Pierce, C.L., Corcoran, A.M., Gronbach, A.N., Hsia, S., Mullarkey, B.J., and A.J. Schwartzhoff. 2011. Influence of diel period on electrofishing and becah seining assessments of littoral fish assemblages. Norm. Am. J. Fisher. Manage 21: 918-926.

Rhodes, T.R. 2005. The immediate and short-term impacts of catch-and-release angling on migrating and pre-spawning condition Rainbow Trout (Oncorhynchus mykiss) in the Bow, River, Alberta. Msc thesis, Department of Biological Science, University of Calgary, Calgary Alberta. 239 pp.

Sanders, R.E. 1991. Day versus night electrofishing catches from near-shore waters of the Ohio and Muskingum Rivers. Ohio J. Sci 92: 51-59.

Williams, B.K., Nichols, J.D., and M.J. Conroy. 2002. Analysis and management of animal populations, modelling, estimation, and decision making. Academic Press, San Diego, CA. 817 pp.

6.0 Tables and Figures

Table 1. The number and total length of sites in the Bow River sampled by boat electrofishing based on multiple passes within a year (Mark-Recap) or a single pass (One-Pass). Site length is calculated as the total length of bank that is sampled divided by 2.

	Number of Sites			Total Length of Sites (km)		
Year	**Mark-Recap**	**One-Pass**	**Total**	**Mark-Recap**	**One-Pass**	**Total**
1999	4		4	4		4
2000	4		4	4		4
2001	46	107	153	23	53.5	76.5
2003	4		4	4		4
2005	4		4	4		4
2007	4		4	4		4
2008	4		4	4		4
2011	4		4	4		4
2012	4		4	4		4
2013	8		8	8		8
2017		6	6		6	6
2018	4	12	16	4	12	16
2019		13	13		13	13
2020		13	13		13	13
2021	4		4	4		
Total	94	151	245	71	97.5	164.5

Table 2. Example of mark-recapture data for Rainbow Trout from site 304.5 in 2021 from the 4th size class (300-400 mm). The unmarked catch and marks applied to columns shows the number of unmarked fish caught and the number of new marks applied on each pass. The number of marks available to be recaptured from any pass is the sum of marks applied and recaptured on that pass (e.g., 4 marks applied on pass 2 + 2 recaptures on pass 2 = 6 marks available from pass 2 to be recaptured on later passes 3-5). The columns to the right show the number of recaptures by release pass (p_rel in eqn. 4)) and recovery pass (p_rec).

	Unmarked	Marks	Marks	Recaptures by Pass			
Pass	**Catch**	**Applied**	**Available**	**2**	**3**	**4**	**5**
1	9	9	9	2	1	1	0
2	5	4	6		1	1	0
3	10	10	12			3	0
4	6	6	11				0
5	8	NA	NA				

Table 3. The number of marked fish recaptured in sites other than the one they were released in for Brown Trout (BNTR), Mountain Whitefish (MNWH), and Rainbow Trout (RNTR). Also shown are the total number of RNTR recaptures (across-site + within-site) and the expected values of year-specific movement-related mark loss rates for RNTR assuming they are independent values (θ_y = across-site recaptures/total recaptures).

	Across-Site Recaptures			Total Recaptures	
Year	**BNTR**	**MNWH**	**RNTR**	**RNTR**	θ_y
1999	6	6	2	10	0.20
2000	1	14	8	23	0.35
2001	7		19	47	0.40
2003	2	1	4	39	0.10
2005	3	3	19	57	0.33
2007	6	1	9	31	0.29
2008	3		12	51	0.24
2011	4		5	95	0.05
2012	1	1		37	0.00
2013		1	3	100	0.03
2018	1	3	6	46	0.13
2021	2	1	34	169	0.20
Total	36	31	121	705	0.19

Table 4. Estimates of the standard deviations that determine the extent of year- and site-specific variation in capture probability, and the extent of unexplained process error (see eqn. 1).

Effect	Parameter	Mean	95% Interval
Year	σ_y	0.40	0.19 - 0.77
Site	σ_s	0.28	0.05 - 0.64
Process error	σ_p	0.59	0.53 - 0.64

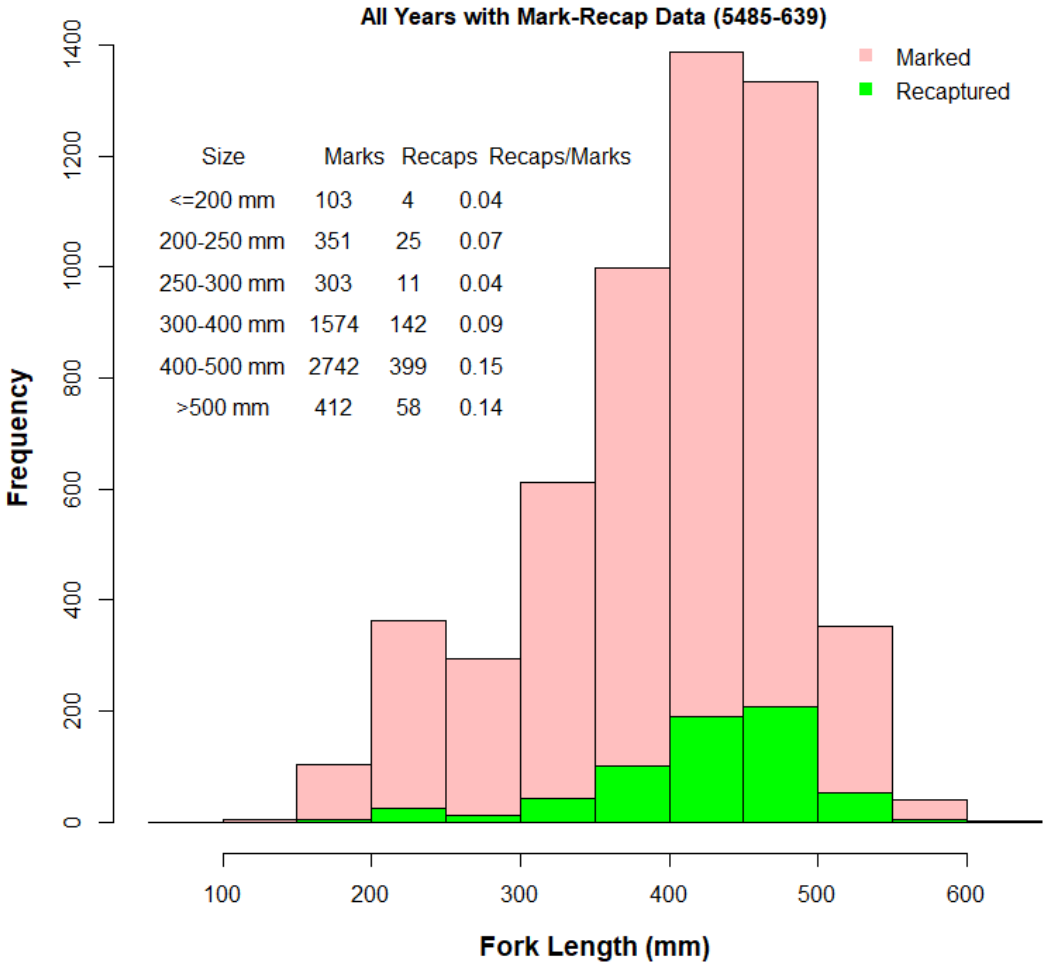

Figure 1. Histogram of the number of Rainbow Trout captured and marked at mark-recapture sites over the 1999-2021 study period (pink), and the number of recaptures (green). Text on the plot shows the number of marks released and recaptured by the six size classes used in the abundance model. The ratio of recaptures/marks is also provided which is a rough estimate of capture probability by size class. The numbers in parentheses at the top of the panel shows the total number of marked fish and the total number of recaptures across size classes.

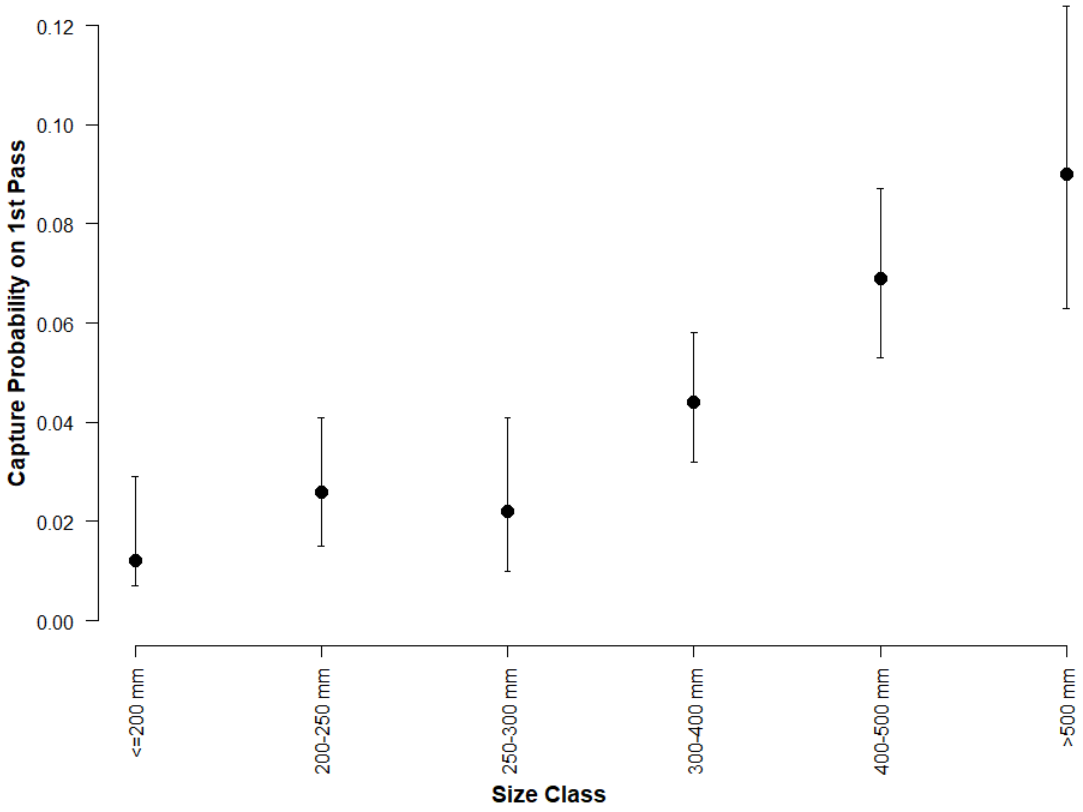

Figure 2. Estimates of capture probability by size class on the first pass (transformed β_1 estimates from eqn. 1). Points and error bars represent the median and 95 % credible intervals.

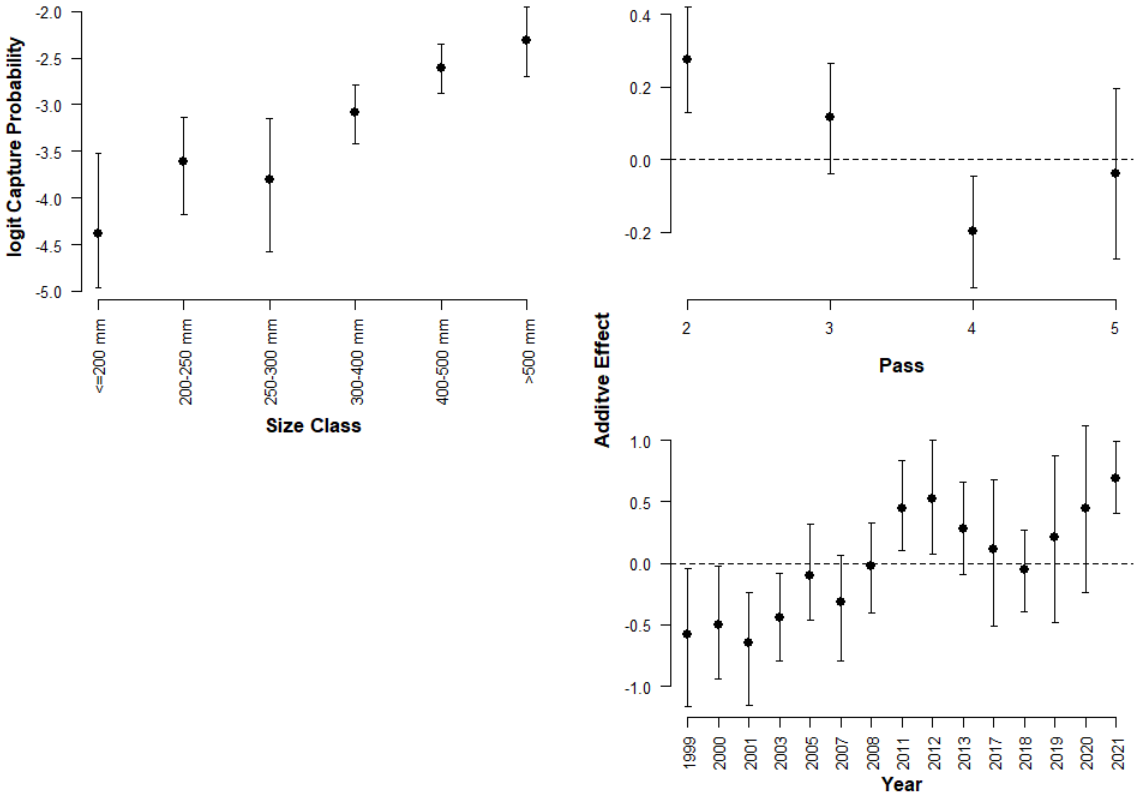

Figure 3. Estimates of size-specific capture probability in logit space (β_l, top-left panel) and pass (β_p, upper-right panel) and year (β_y lower-right panel) additive effects. Points and error bars represent the median and 95% credible intervals.

a) Mark-recapture sites only

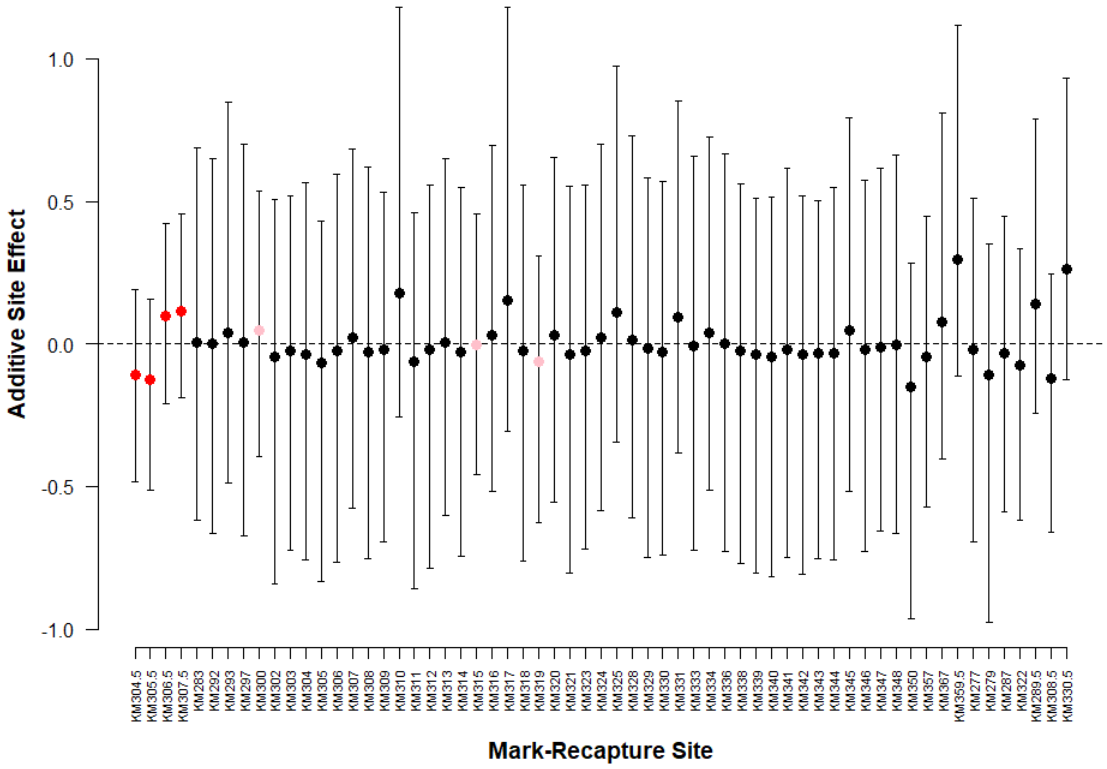

Figure 4. Estimates of site effects on capture probability (β_s) in logit space. Panel a) shows estimates for mark-recapture sites only, with red, pink, and black points identifying sites sampled 8-9 times, 2 times, or only 1 time across all study years, respectively. Panel b) shows estimates for all sites sampled over all study years, with red and black points identifying sites sampled by mark-recapture and one-pass, respectively.

b) All sites

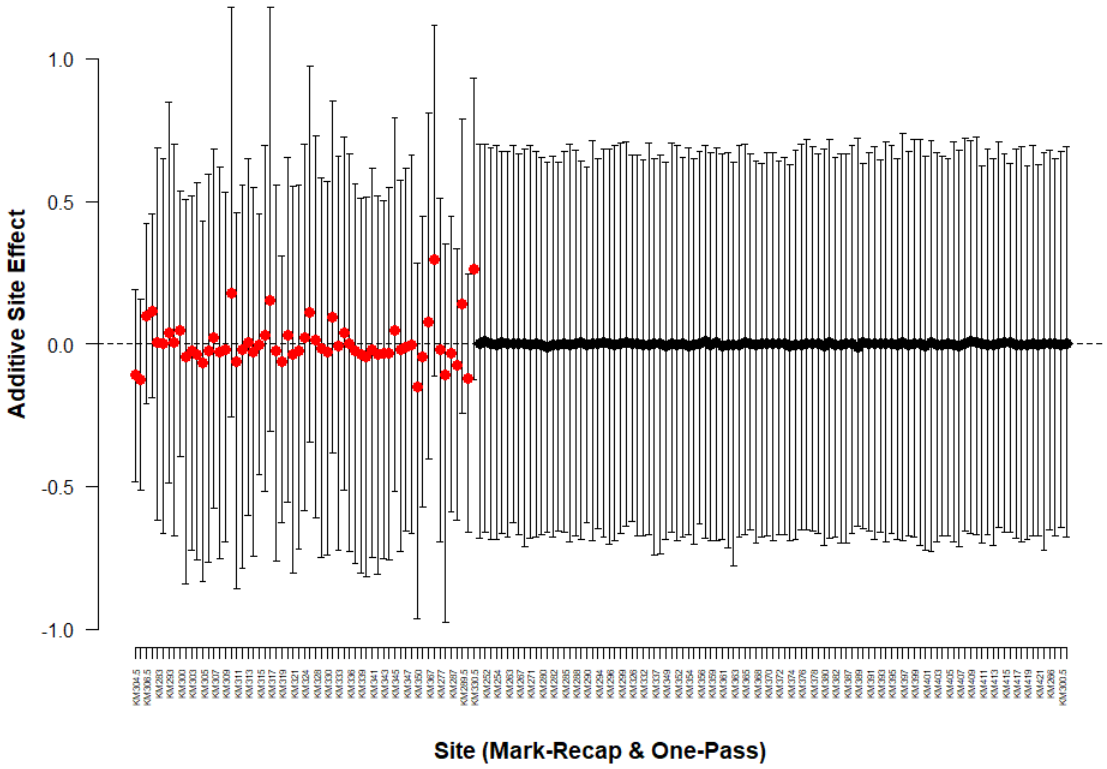

Figure 4. Con't

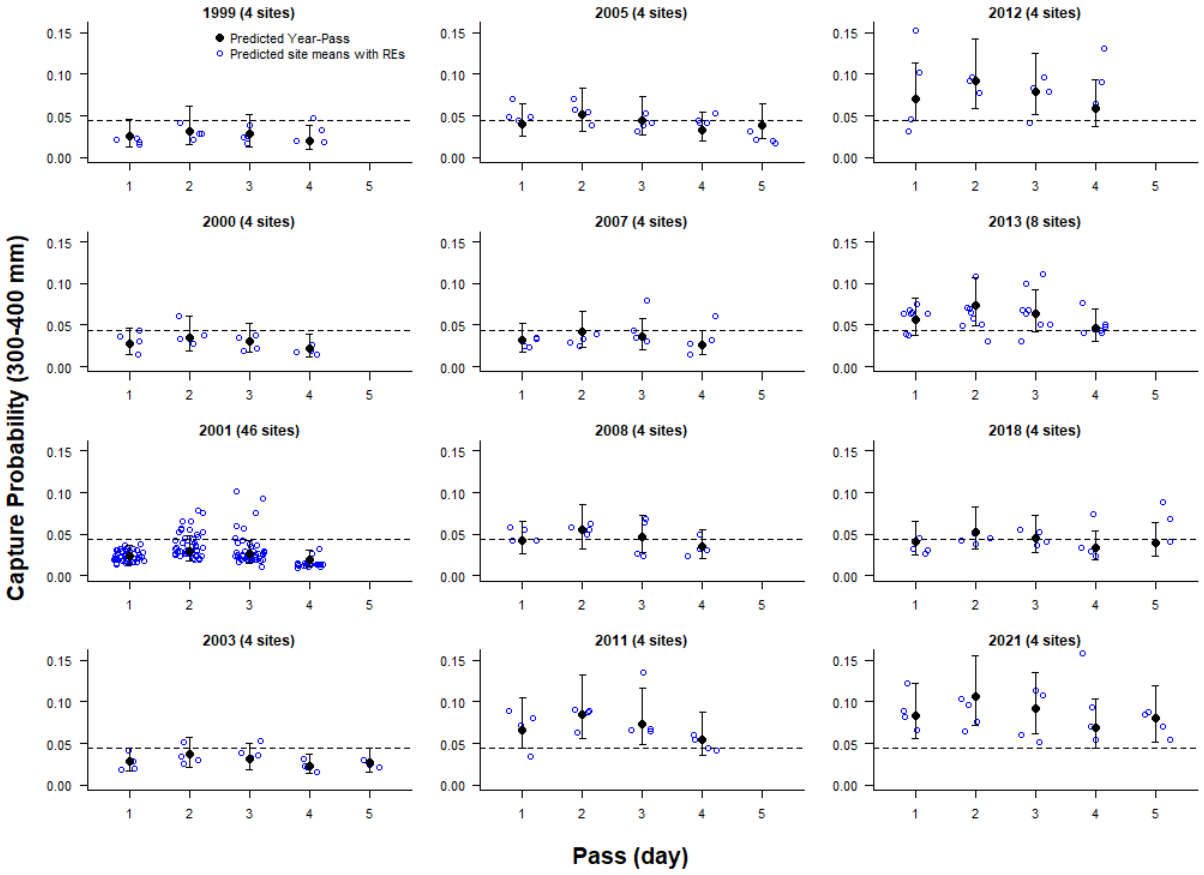

Figure 5. Capture probability estimates for the 300-400 mm size class by year (panel) and pass (x-value). The black points and error bars represent the median and 95% credible intervals based on transformed values $\beta_{p=4} + \beta_p + \beta_y$ in eqn. 1. The open blue points represent the estimates by site, and thus include the additional effect of β_s as well as the process error $\varepsilon_{y,s,p,l}$. The dashed horizontal line shows the across-year mean capture probability for the size class on pass 1.

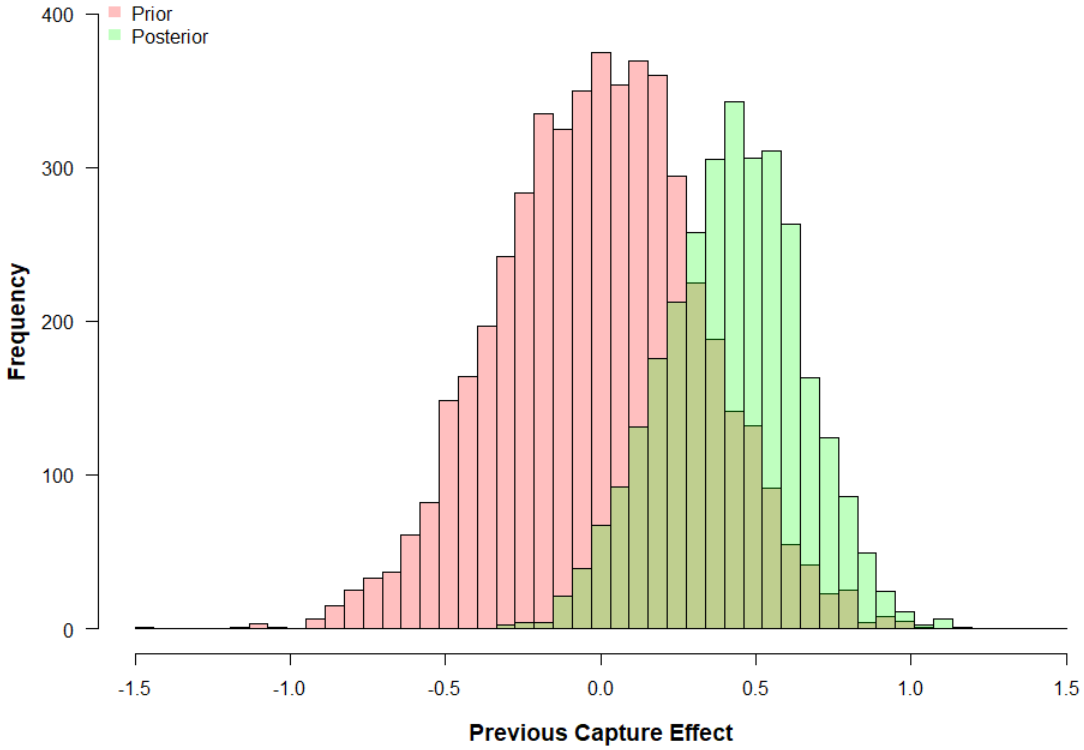

Figure 6. Prior and posterior distributions for the effect of previous capture on later capture probabilities (γ). The olive-green shaded area represents the overlap between prior and posterior distributions.

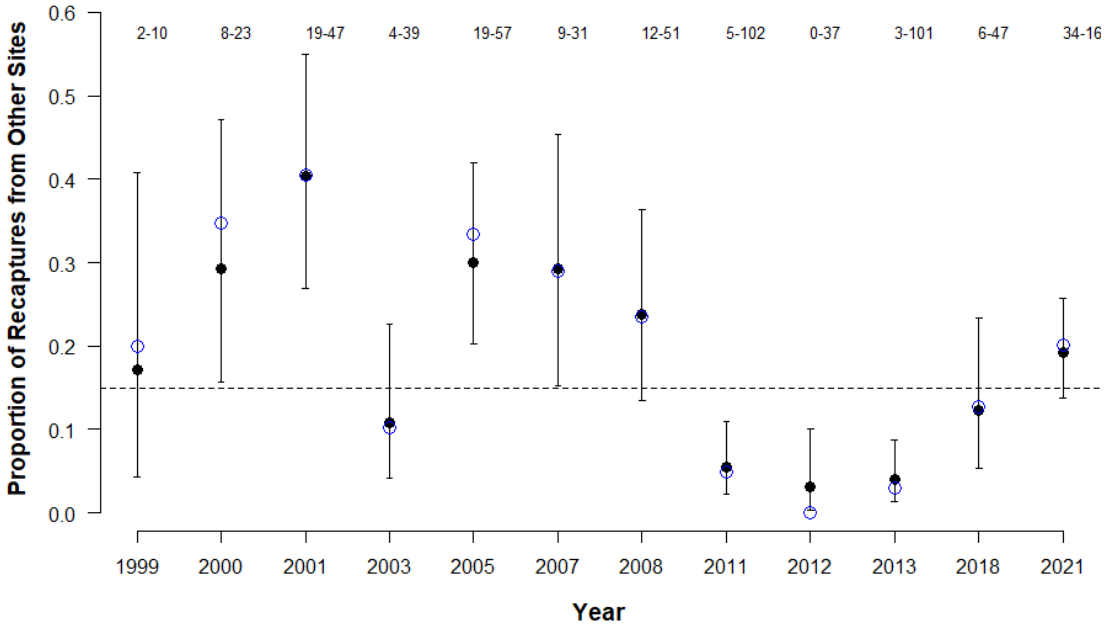

Figure 7. Estimates of the proportion of recaptured fish caught in sites other than the one they were originally marked in, by sampling year (θ_y). The black points and error bars show the medians and 95% credible intervals of θ_y estimates from the model. The black dashed horizontal line shows the transformed median estimate for the mean of the hyper-distribution for θ_y (μ_θ). Blue open points show independent estimates of θ_y (right column of Table 3). The text at the top of the panel shows the number of across-site recaptures and the total number of recaptures by year. The ratio of the two values is the expected independent estimate of θ_y (blue points).

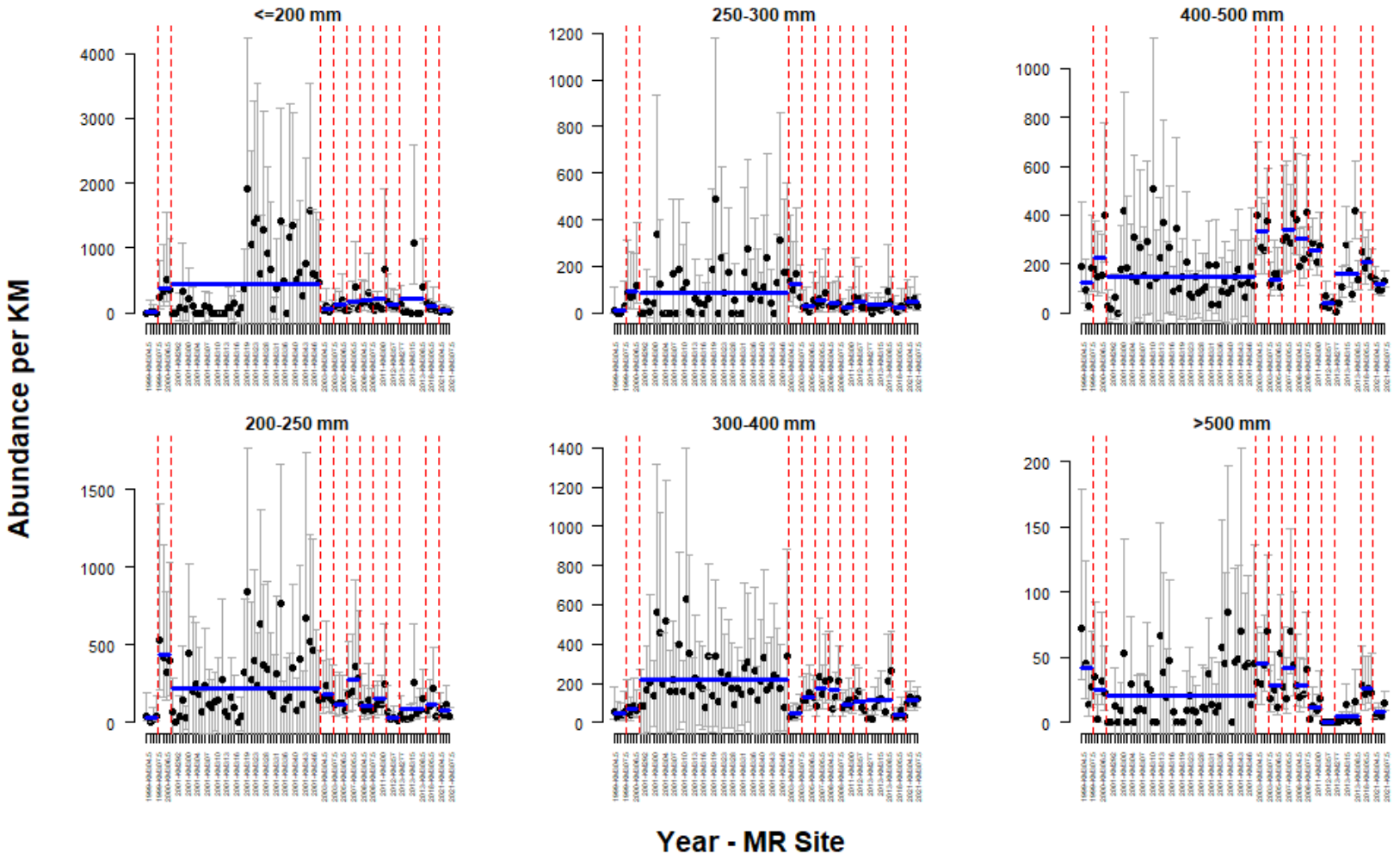

Figure 8. Site-specific estimates of abundance by size class (panels) for mark-recapture (MR) sites. Black points and error bars show the median and 95% credible intervals of estimates. Red dashed vertical lines separate the study years. Horizontal blue lines show the medians of the annual abundance estimates based on data from mark-recapture sites only.

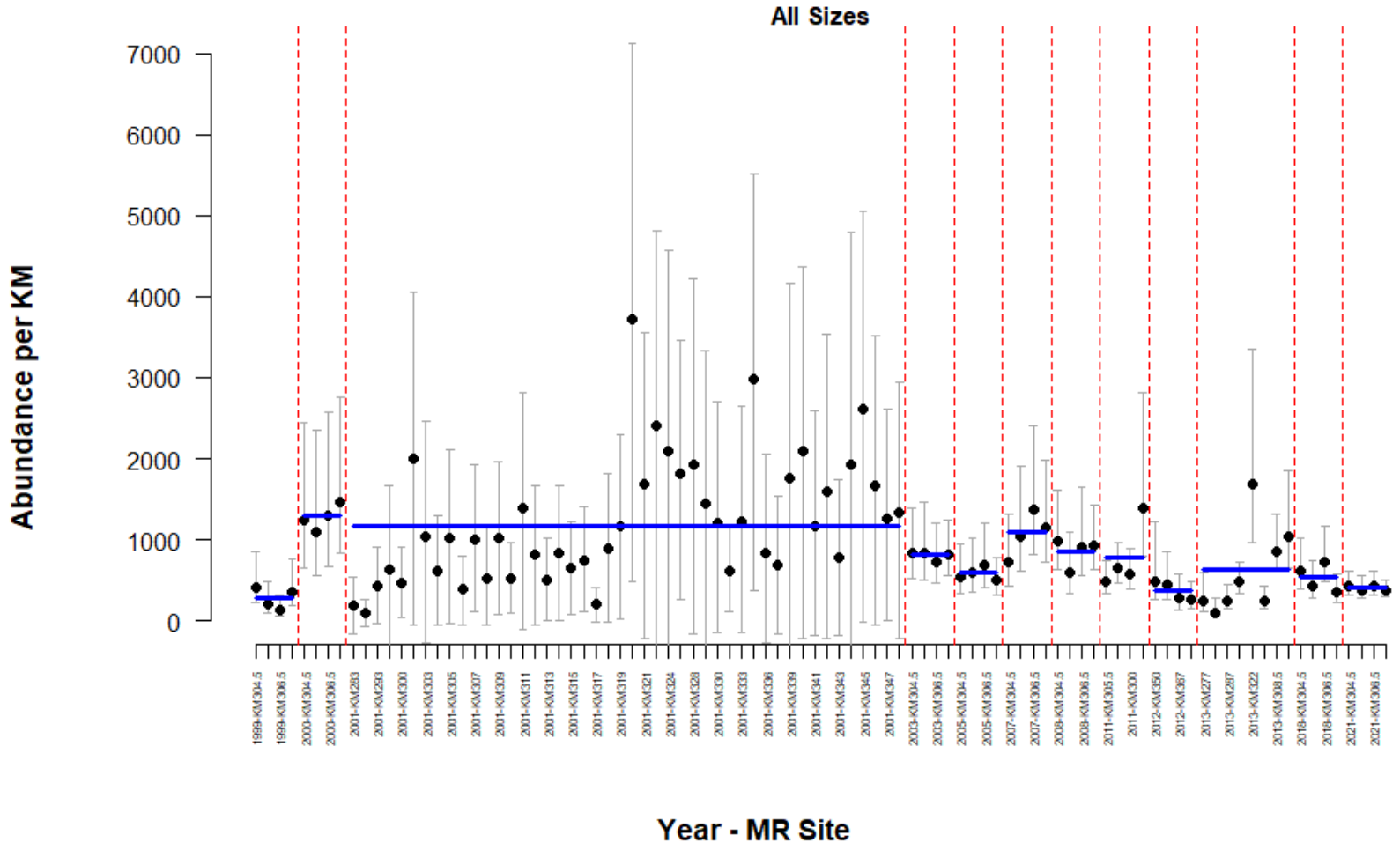

Figure 8. Con't

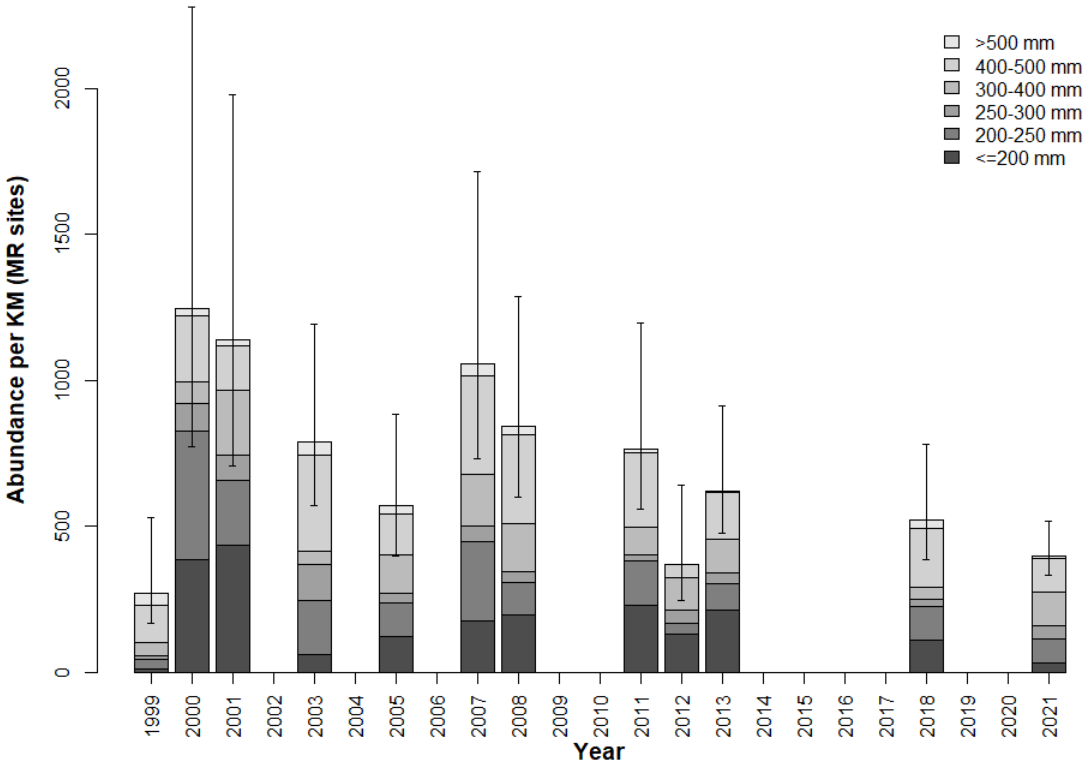

Figure 9. Annual estimates of abundance based on data from only mark-recapture sites. The height of each bar and the error bars represent the median and 95% credible interval of the total abundance across size classes. Shaded bars show the median abundance of each size class.

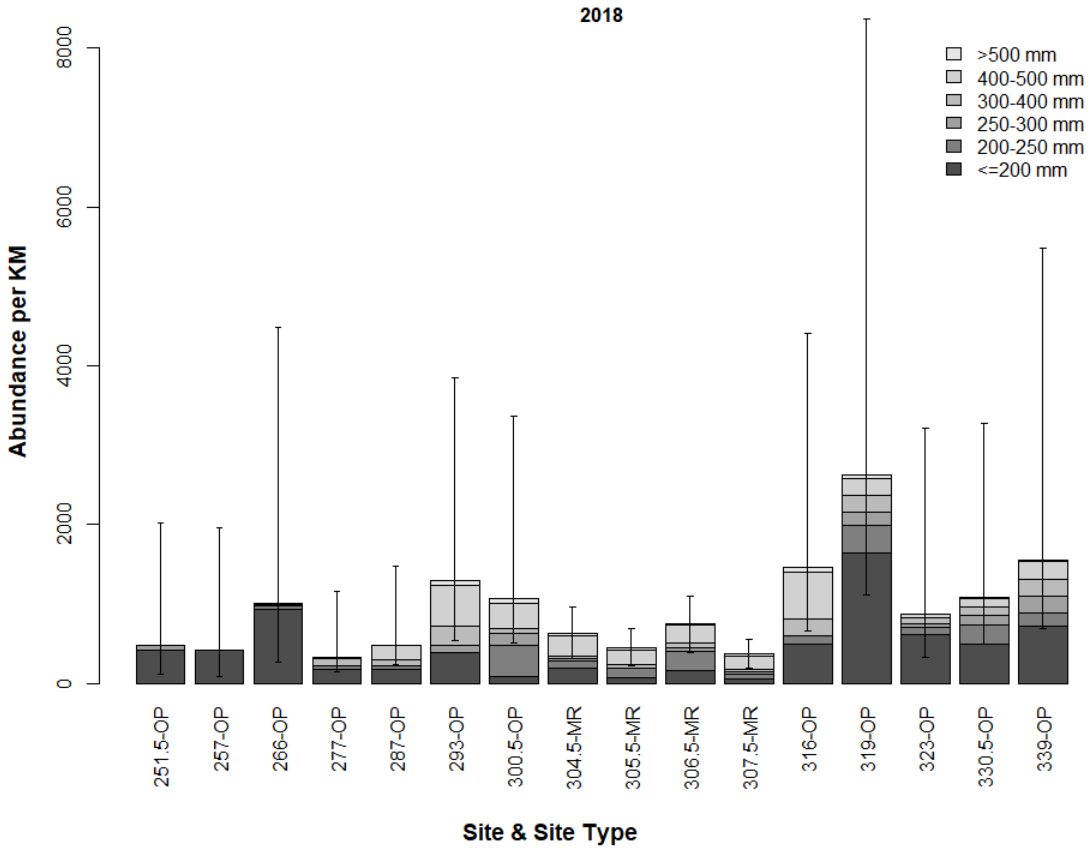

Figure 10. Comparison of abundance estimates by site and site type (mark recapture (MR) and one-pass (OP)) in 2018. See caption for figure 9 for additional details.

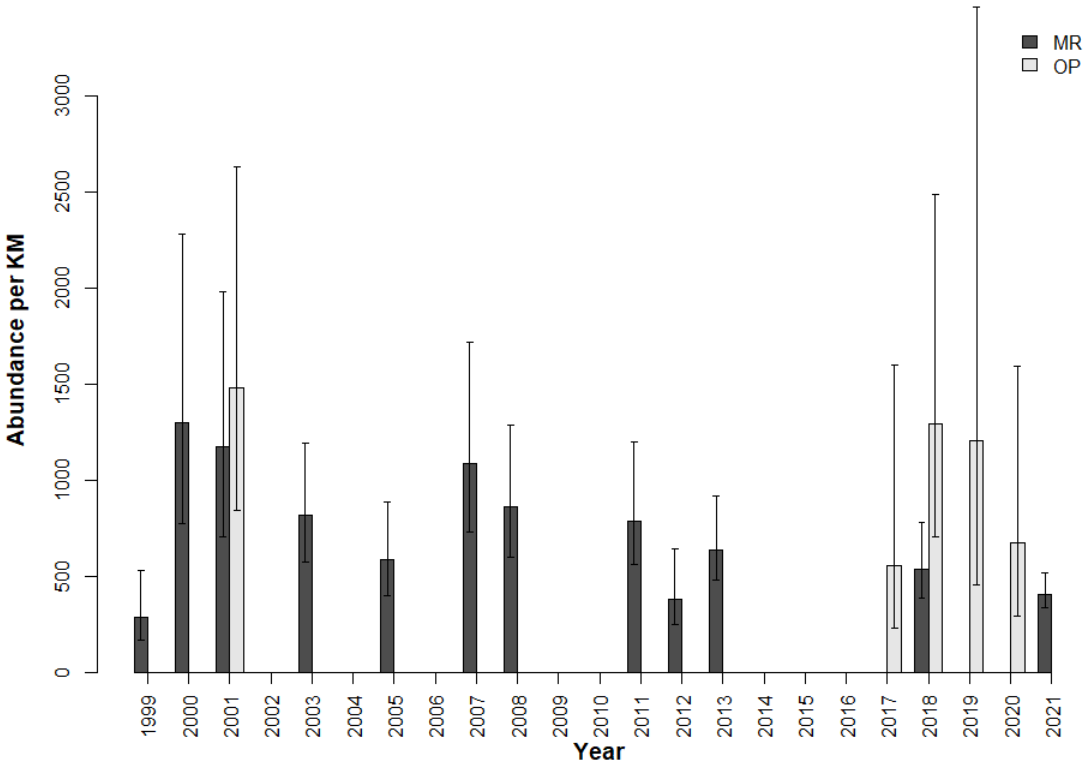

Figure 11. Comparison of size-aggregated annual abundance estimates based on data from mark-recapture (MR, dark bars) and one-pass (OP, open bars) sites. The height of the bars and the error bars represent the median and 95% credible intervals, respectively.

a) No previous capture effect

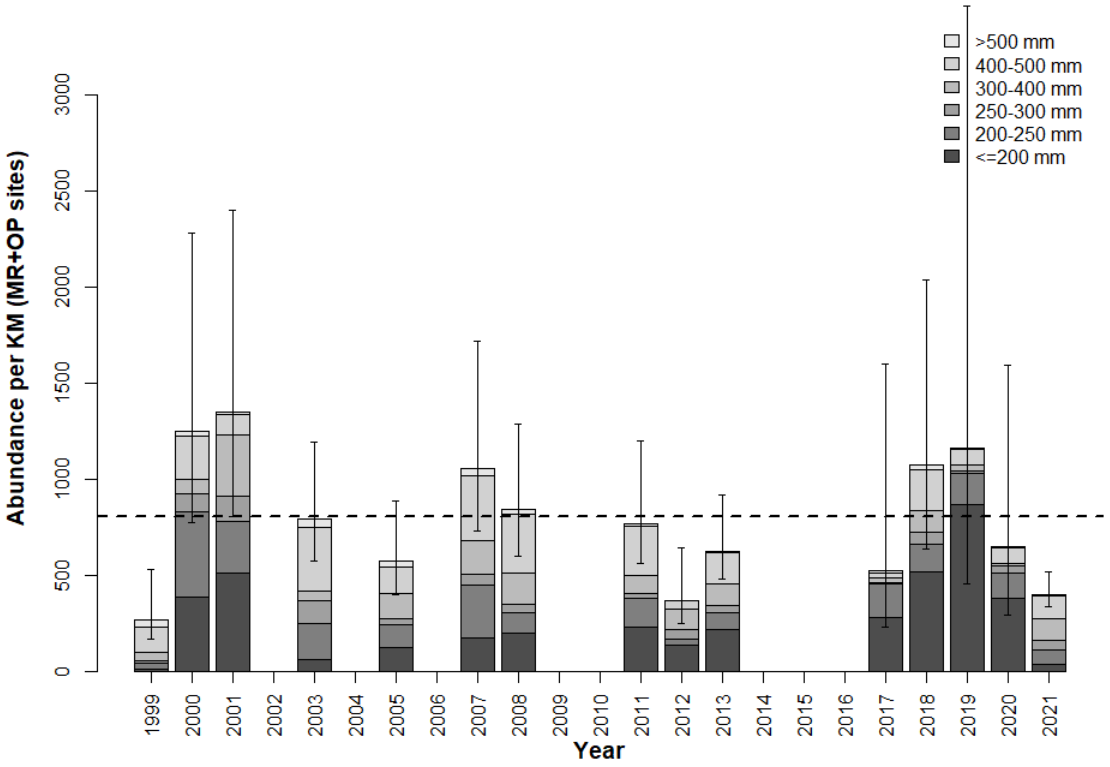

Figure 12. Annual abundance estimates based on all available data for each year (mark-recapture (MR) only, one-pass (OP) only, or mark-recapture and one-pass, see Table 1) without (a) and with (b) an effect of previous capture on capture probability. Results in a) assume capture probability of previously captured and fish not previously captured (unmarked) fish are equal, while b) allows their capture probabilities to differ. The dashed horizontal line represents the interannual mean of size-aggregated annual abundance estimates. See caption for figure 9 for additional details.

b) With previous capture effect

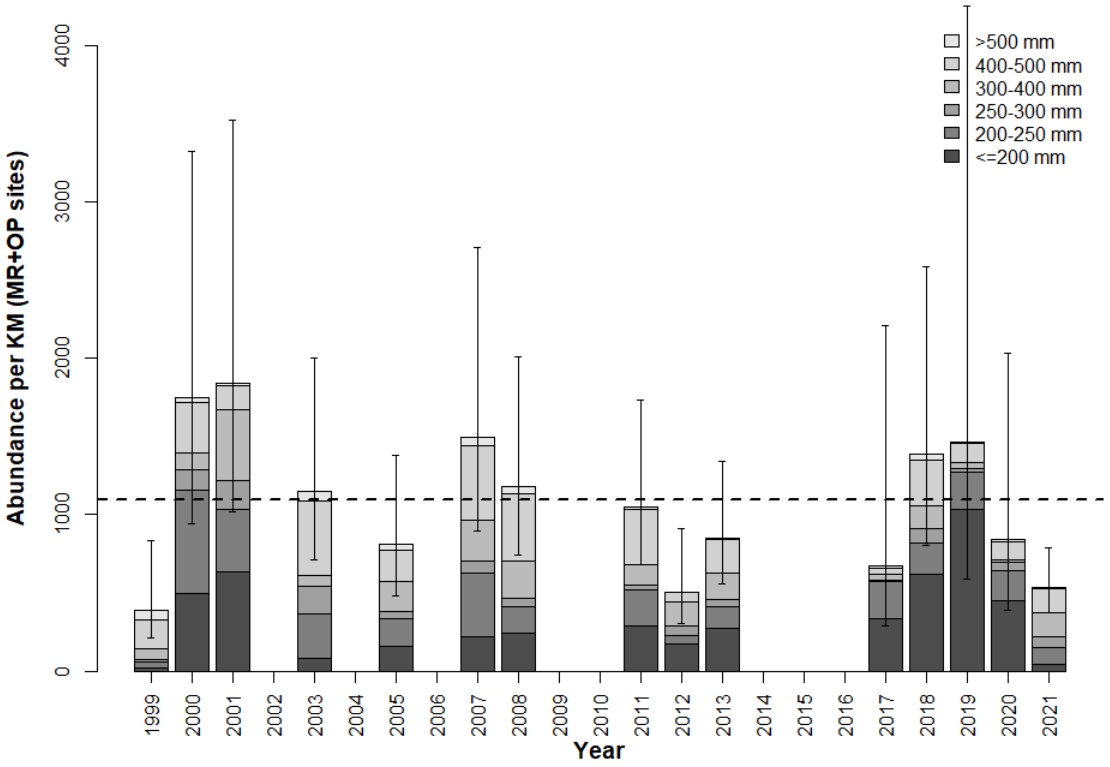

Figure 12. Con't.

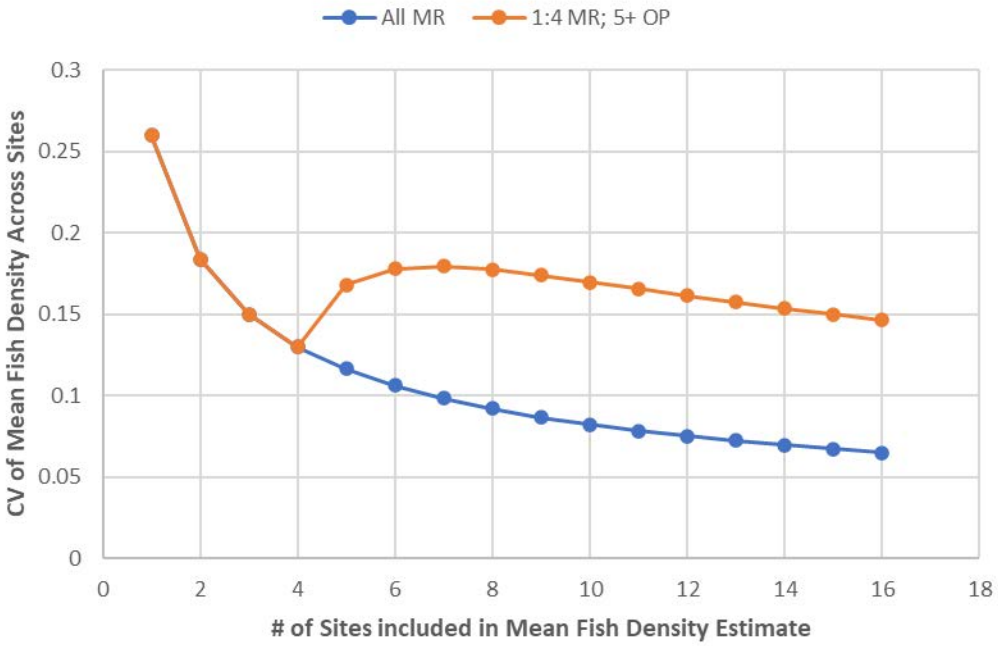

Figure 13. The coefficient of variation (CV) in size-aggregated annual abundance estimates as a function of the number of sites used to calculate the annual estimate. The first scenario (blue line) assumes all sites are sampled by mark-recapture and that the CV of site-specific estimates is 0.26 (mean of 2018 mark-recapture site CV's for size-class aggregated abundance). The second scenario assumes the first four sites are sampled by mark-recapture with the remaining ones sampled by one pass of electrofishing effort (orange line). The assumed CV of one-pass site abundance estimates was set at 0.66, the average CV for one-pass sites sampled in 2018.

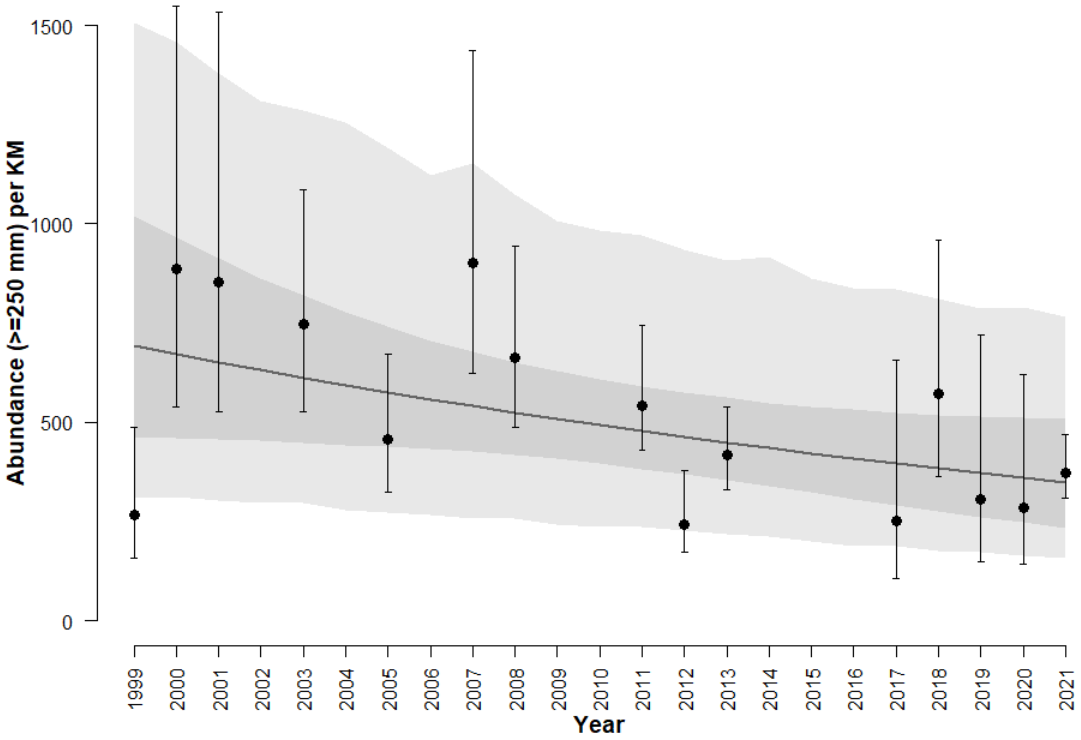

Figure 14. Trend in abundance for rainbow trout ≥250 mm. Points and error bars show the median and 95% credible intervals of abundance estimates from the closed population model. The solid sloping line is the median estimate of the abundance trend. The dark gray shaded area represents the 95% credible interval of the trend based on uncertainty in its parameters (λ_0 and λ). The light gray band represents the 95% credible interval that accounts for both parameter uncertainty in the trend and process error (true year-to-year variation in abundance around the trend line).

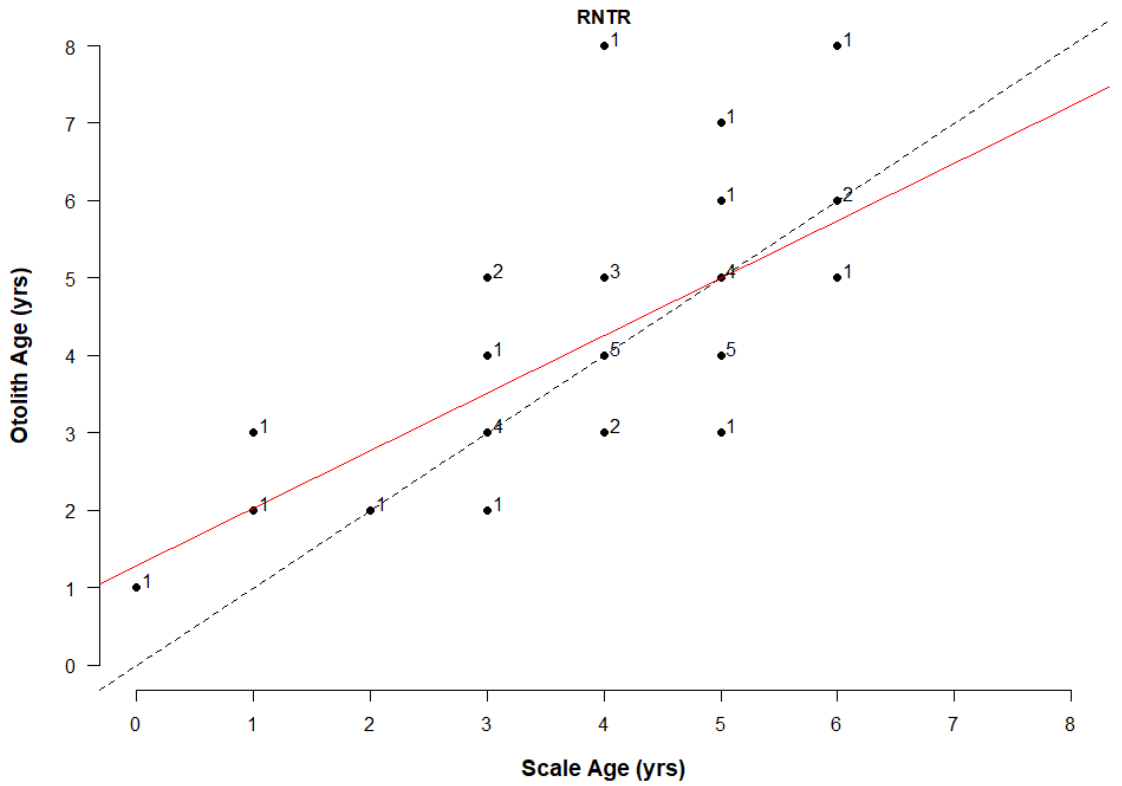

Figure 15. Comparison of age estimates for individual Rainbow Trout based on scale and otolith reads. Numbers beside each point show the sample size. The dashed line is the 1:1 line (scale age = otolith age). The red line is the best-fit regression.

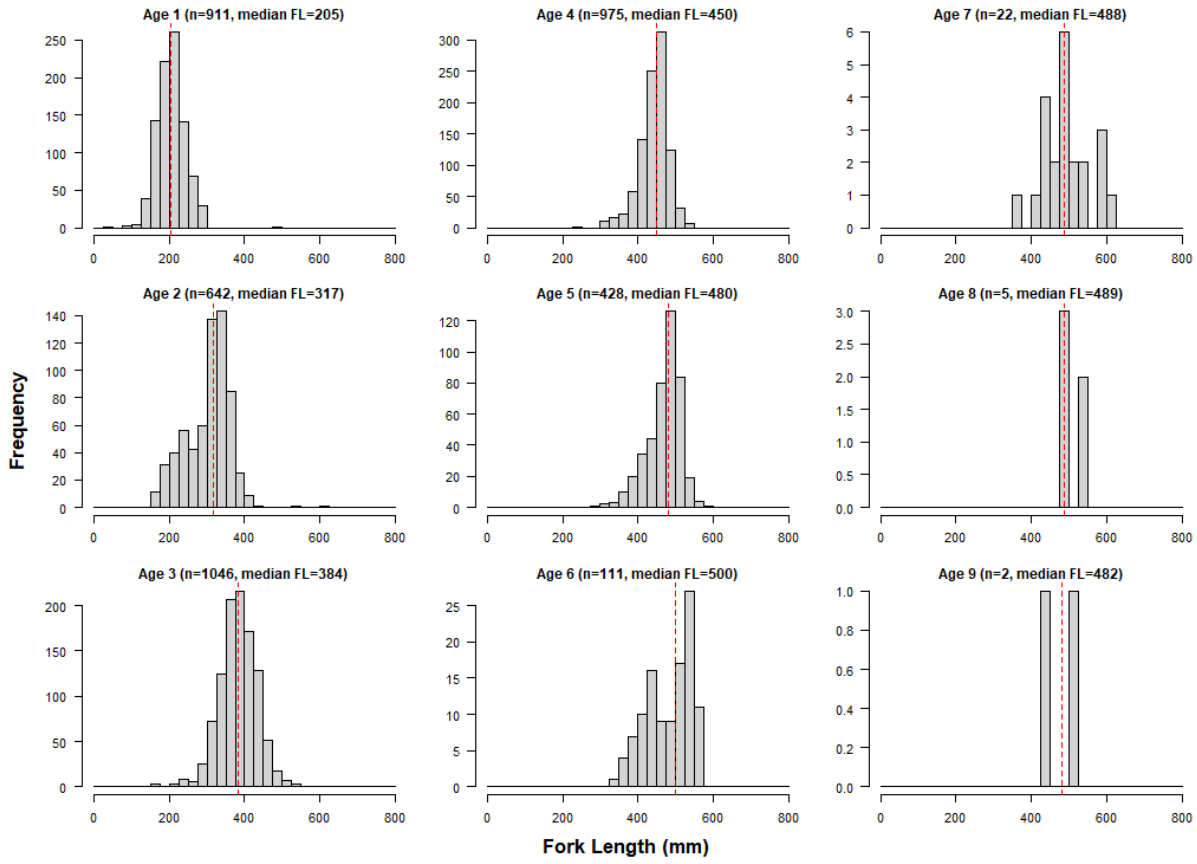

Figure 16. Histograms of Rainbow Trout fork length by age. Vertical red lines denote median fork length for each age. Numbers in parentheses show sample size.

a) Age 1 vs Age 2

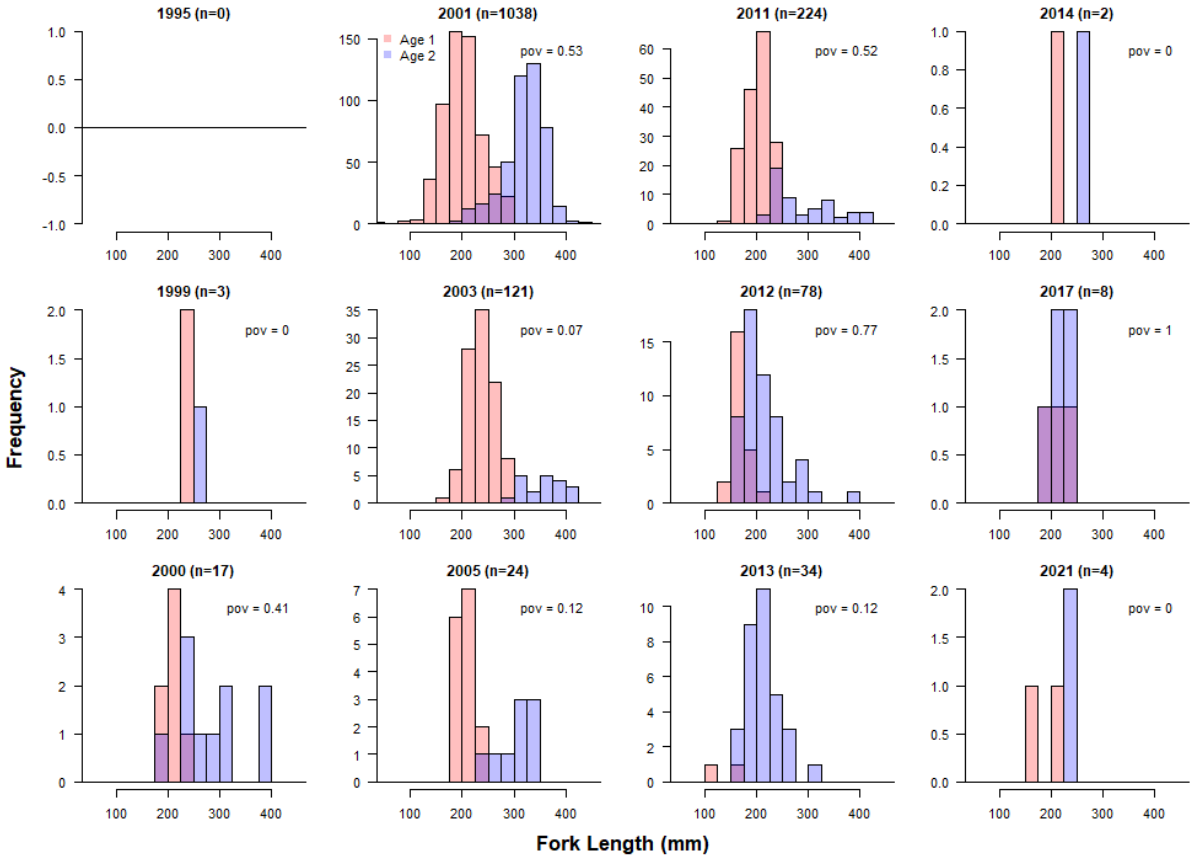

Figure 17. Histograms of Rainbow Trout fork length for some adjacent ages by year of collection. Numbers in parentheses of the panel title shows the sample size. 'pov' is the proportion of the total sample size in 50 mm fork length classes where both age classes were observed (i.e., overlapping size classes identified by purple bars).

b) Age 2 vs Age 3

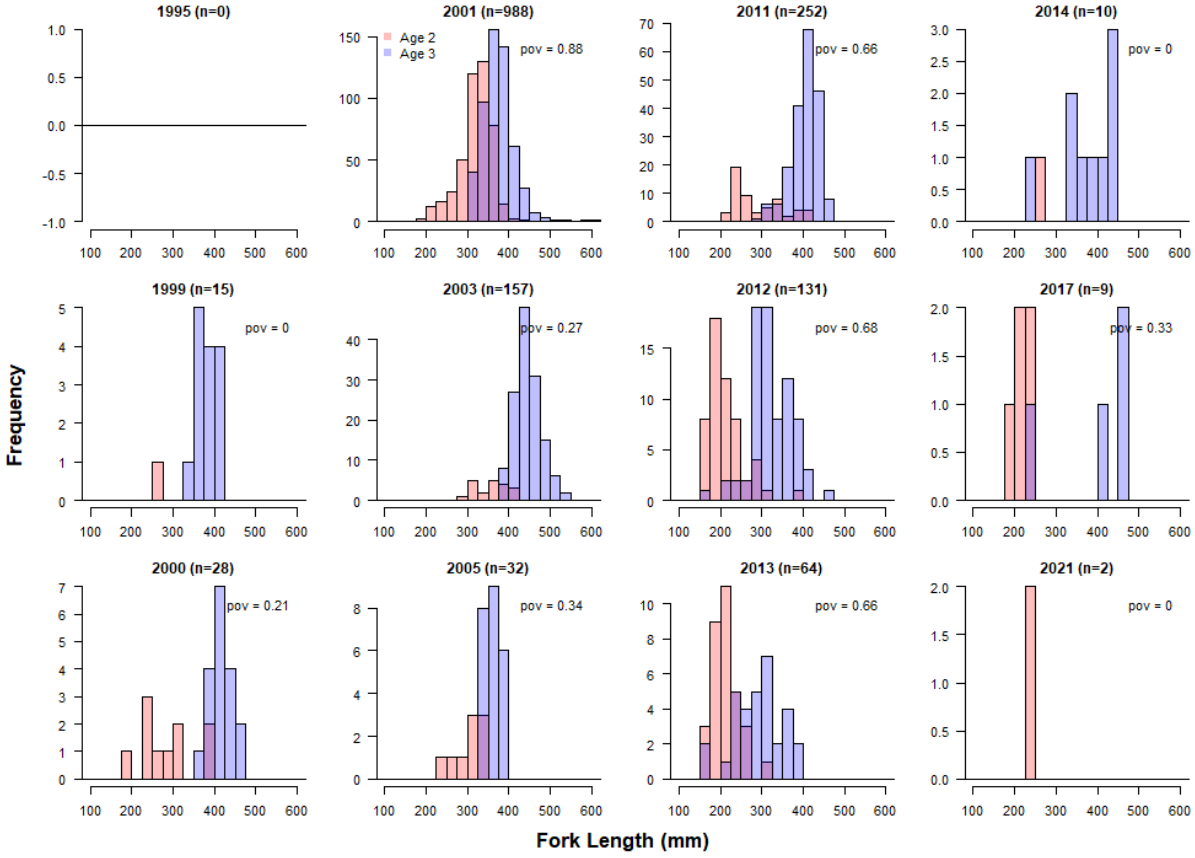

Figure 17. Con't.

c) Age 3 vs Age 4

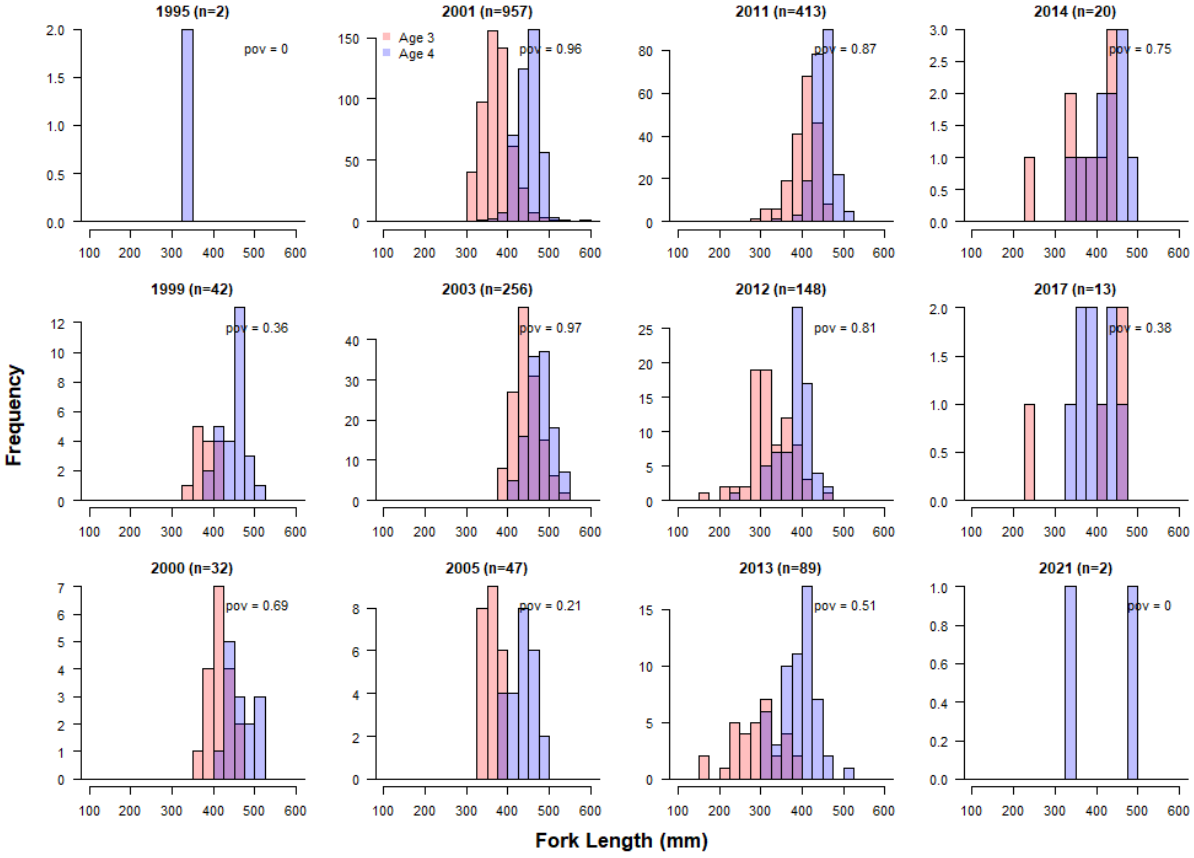

Figure 17. Con't.

a) Predictions and data

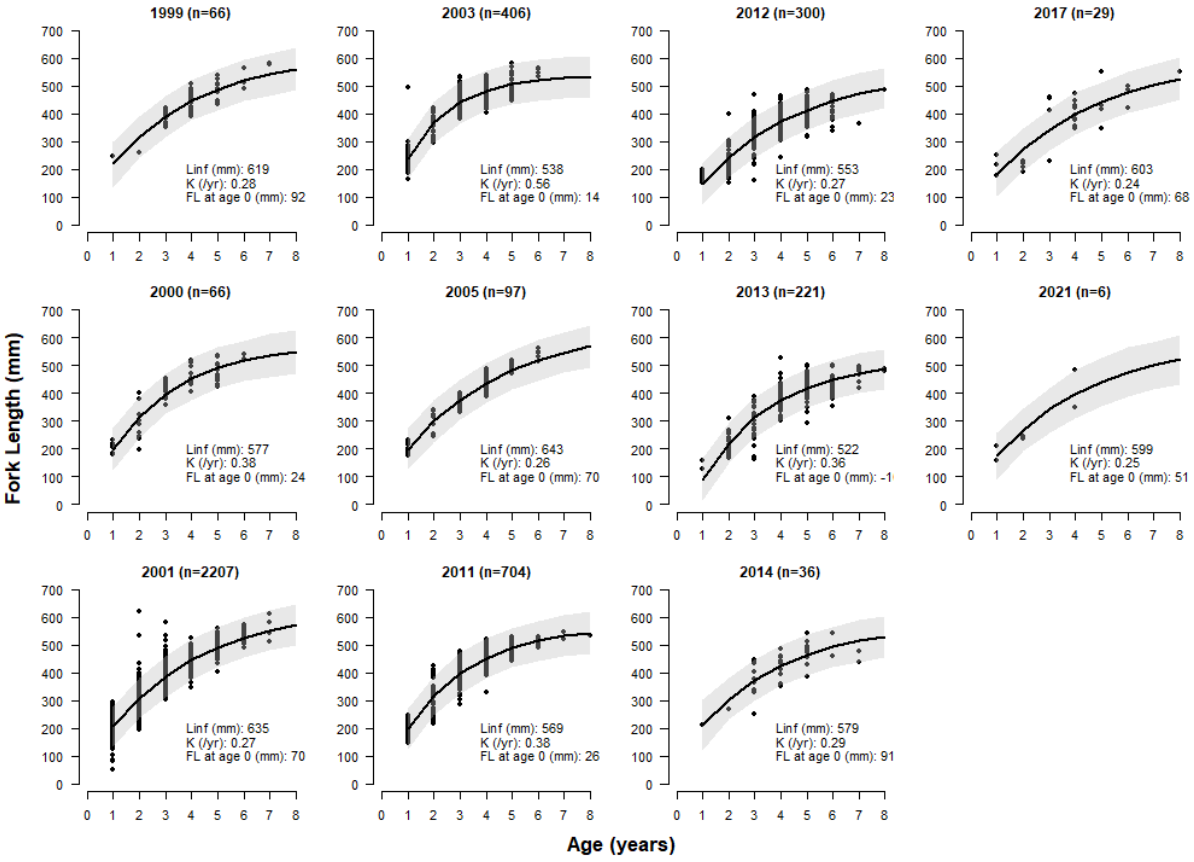

Figure 18. Estimated von Bertalanffy length-age relationships for Rainbow Trout by collection year (a). Points show the observed fork length and age determinations. The solid lines show the median size-at-age estimates predicted from year-specific von Bertalanffy models (parameters shown in text on each panel) fit to the data, and the grey bands show the 95% credible intervals in predicted size-at-age. The numbers in parentheses in the panel titles show the sample size. A comparison of predicted length-age relationships across years is shown in b).

b) Comparison of predictions across years

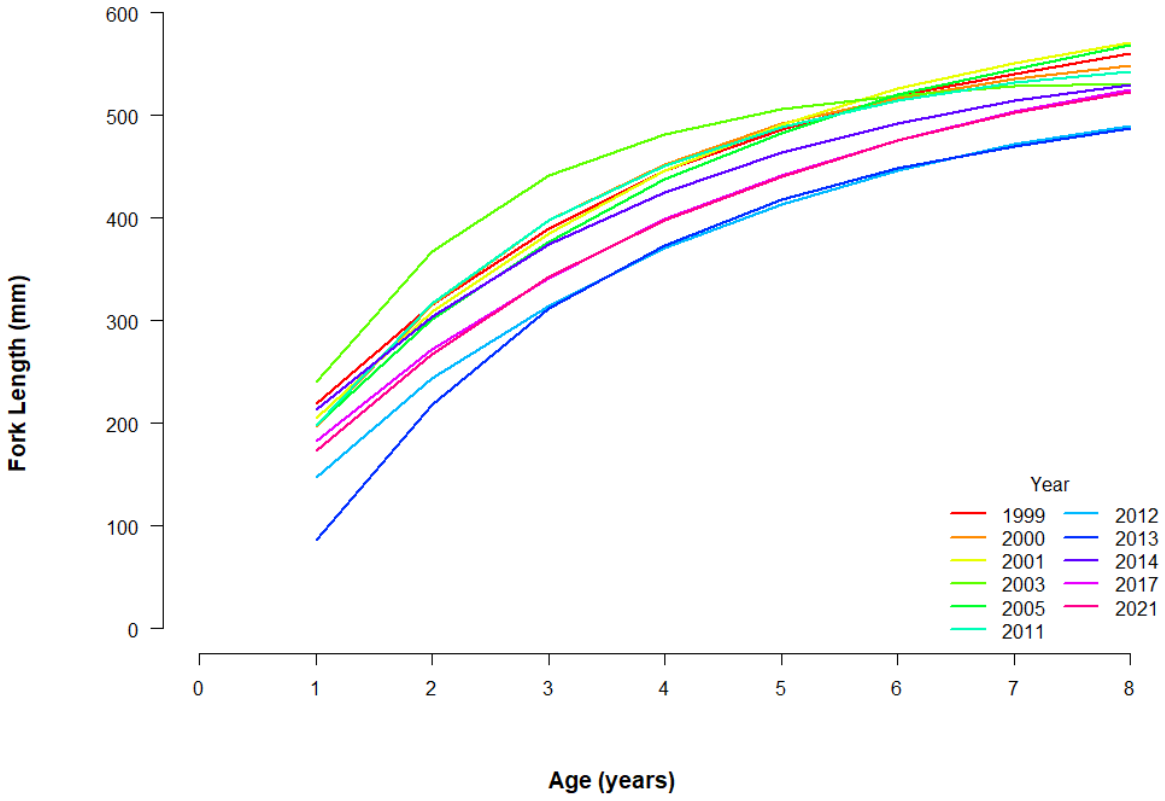

Figure 18. Con't.

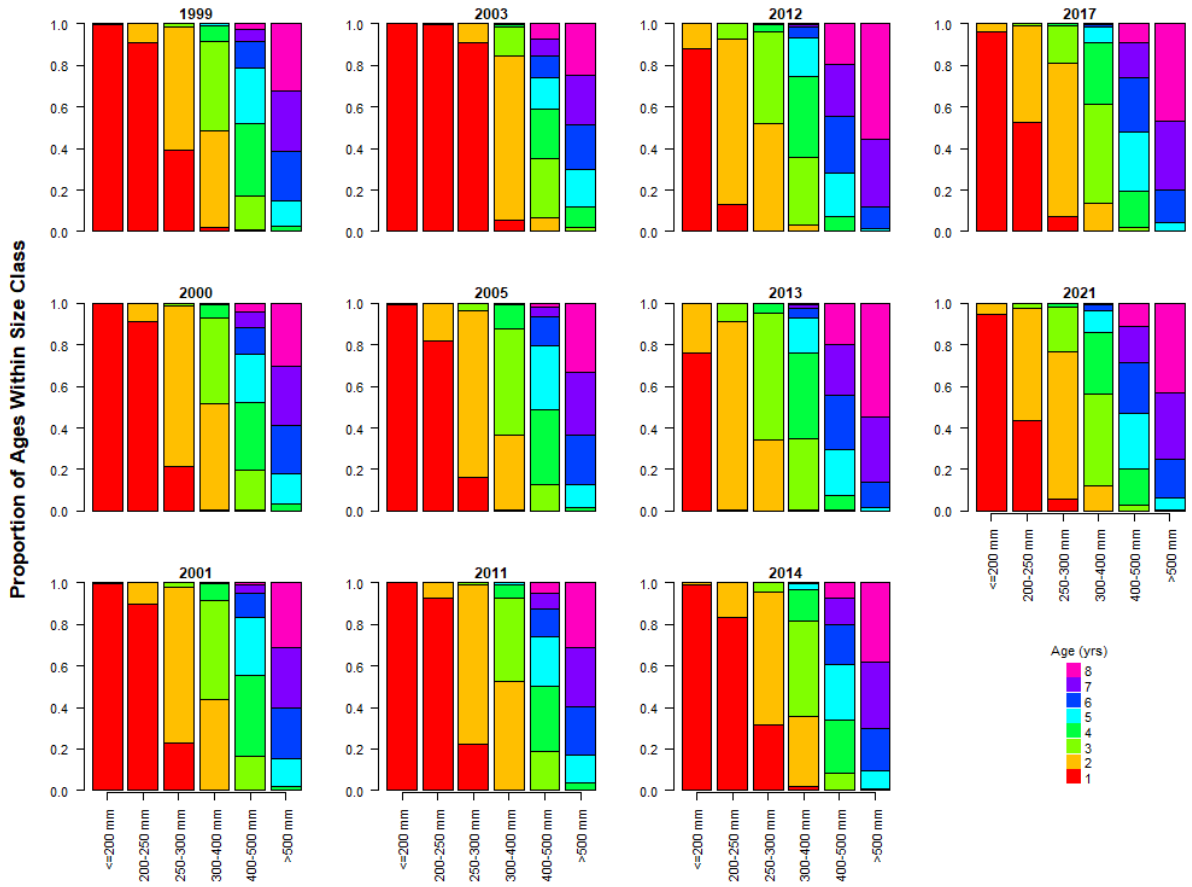

Figure 19. Median predicted proportions of age classes within each fork length size class used in the close population model to estimate annual Rainbow Trout abundance. Proportions are determined based on year-specific von Bertalanffy relationships (Fig. 18) and account for variation in length within ages.

a) 1999 (n=66, small sample size, faster growth)

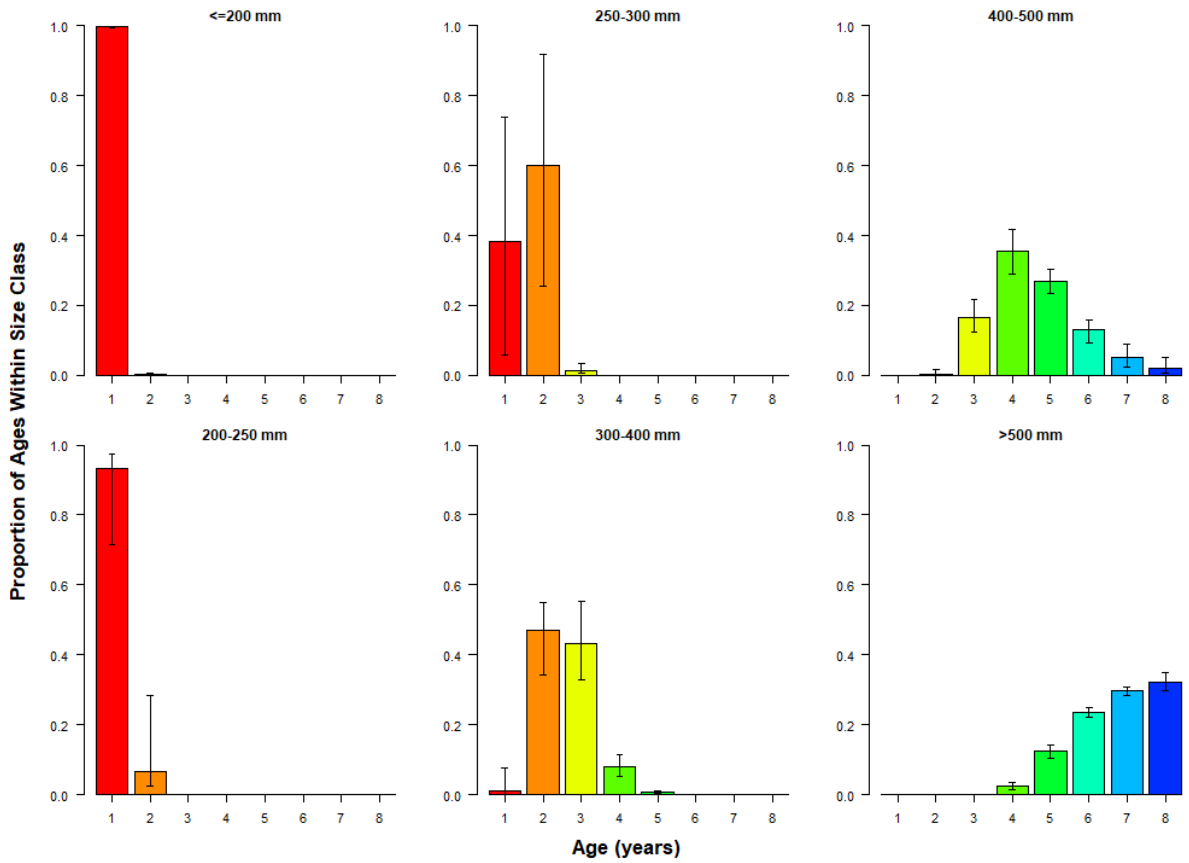

Figure 20. Von Bertalanffy proportions of age classes within each fork length size class used in the closed population model to estimate abundance for 1999 (a) and 2013 (b). Proportions are determined based on year-specific von Bertalanffy relationships (Fig. 18) and account for variation in length within age. Bar heights show median values and error bars show 95% credible intervals. The heights of the bars are the same as the within-age bar heights in figure 19.

b) 2013 (n=221, larger sample size, slower growth)

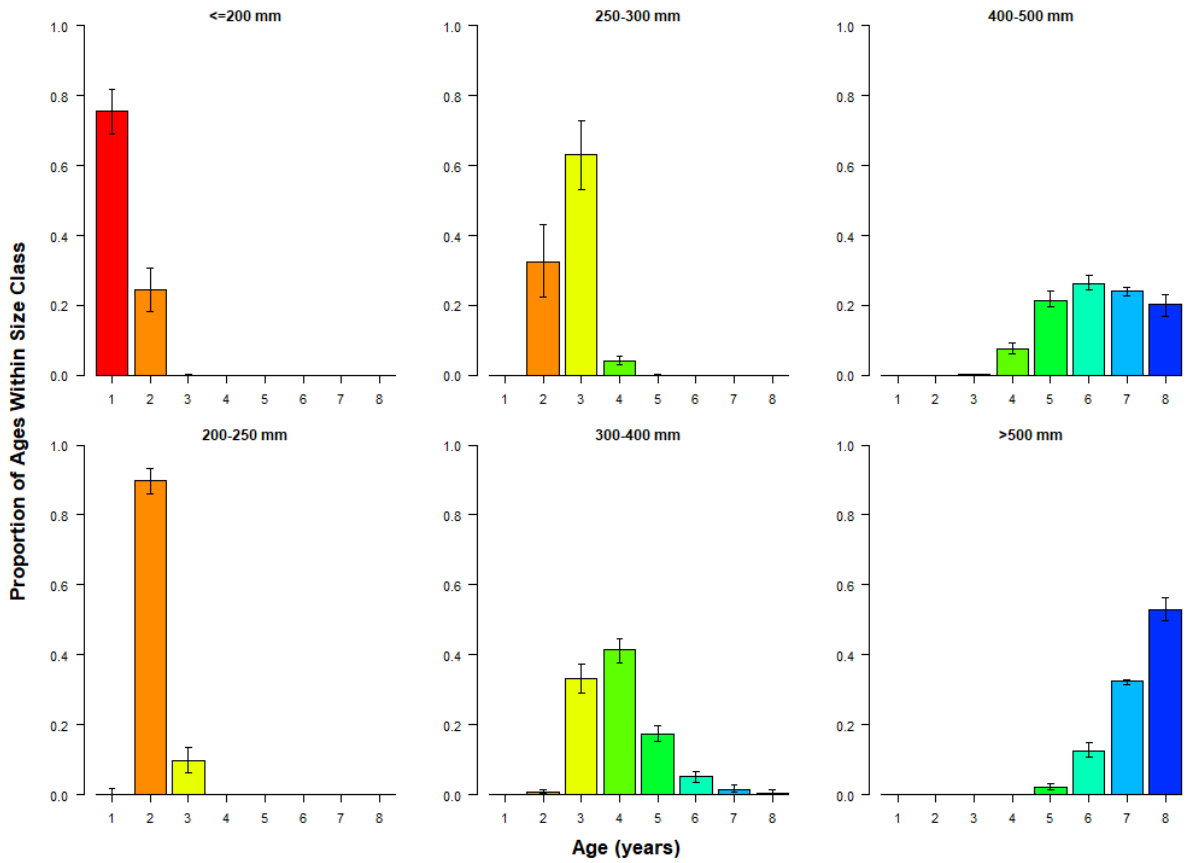

Figure 20. Con't.

a) 1999 (n=66, small sample size, faster growth)

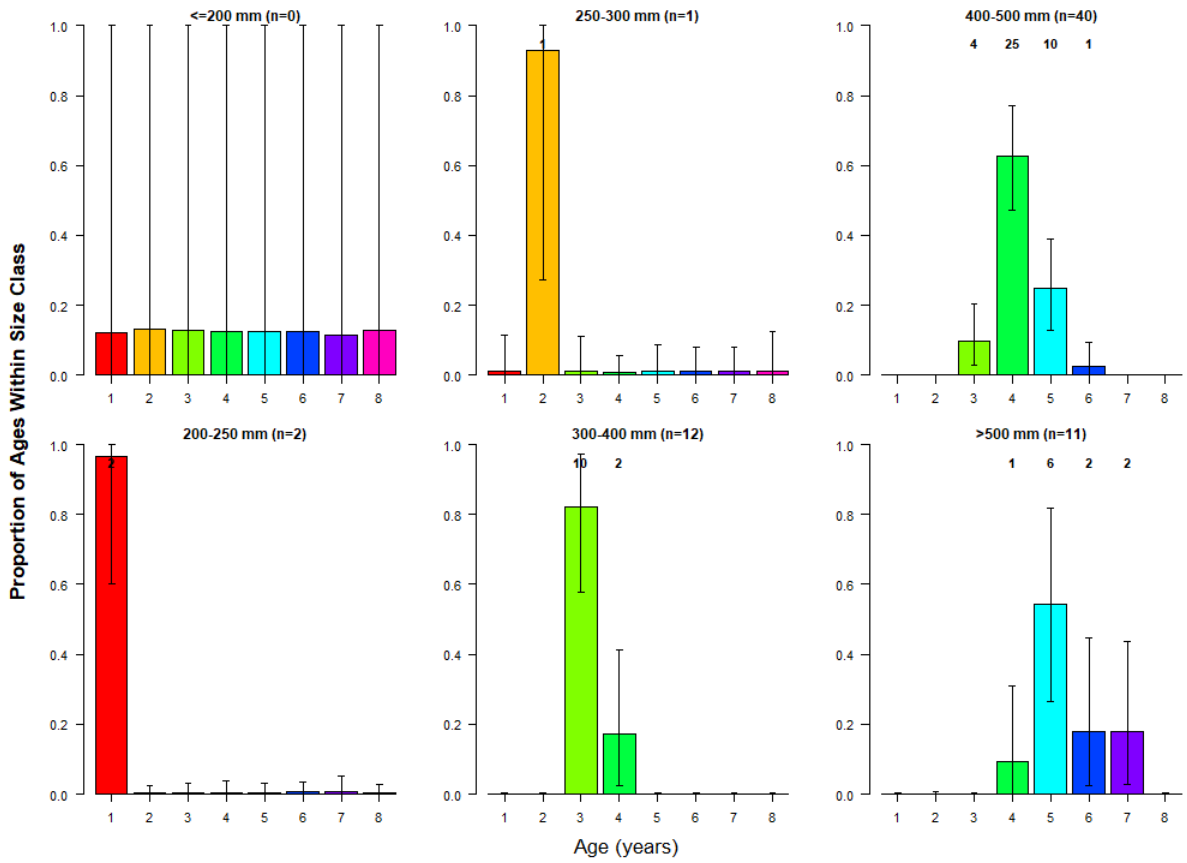

Figure 21. Multinomial proportions of age classes within each fork length size class used in the closed population model to estimate abundance for 1999 (a) and 2013 (b). Proportions are determined based on year- and size class-specific multinomial fits only. Bar heights show median values and error bars show 95% credible intervals. Numbers at the top the bars in each panel are the number of age determinations for each age within the size class, with the total sample size shown in the title in parentheses.

b) 2013 (n=221, larger sample size, slower growth)

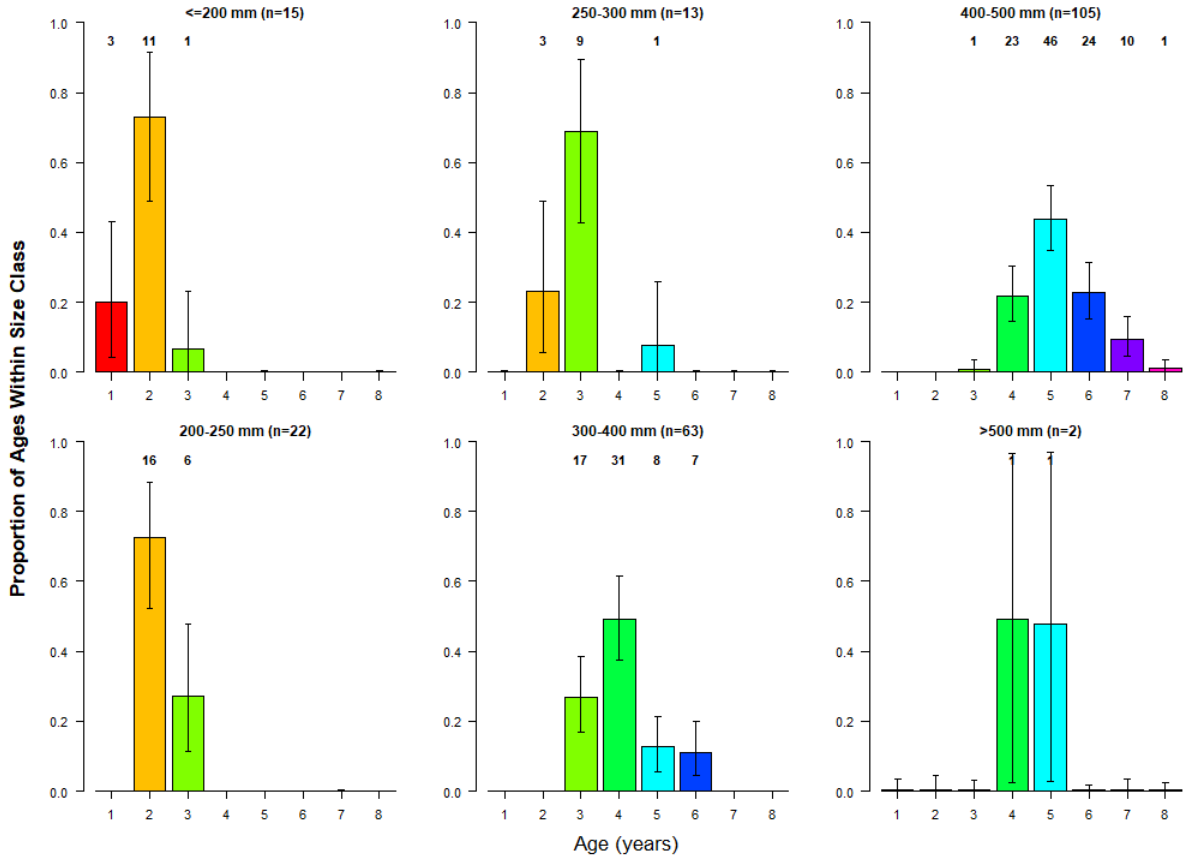

Figure 21. Con't.

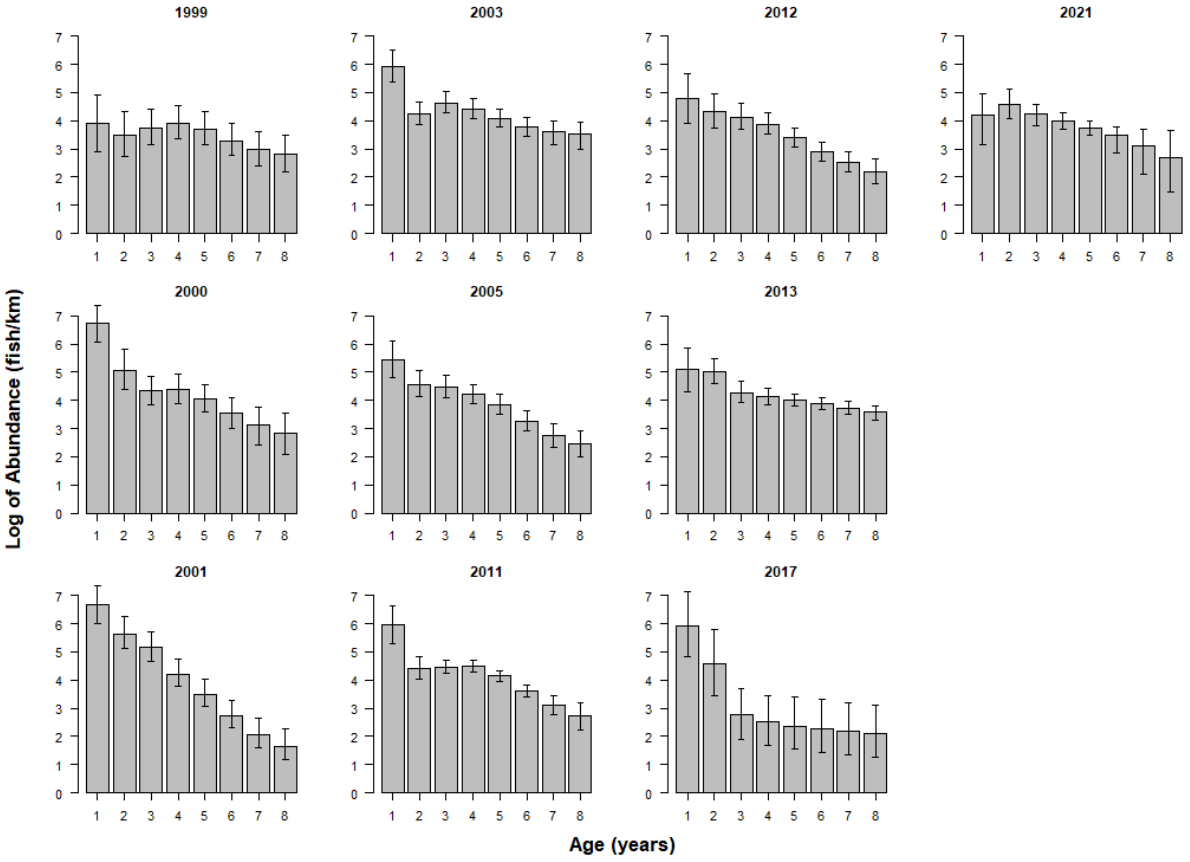

Figure 22. Abundance estimates of Rainbow Trout by age class for years with sufficient ageing data to estimate the proportion of each age class in each size class. The estimated proportions-by-age in each size class (e.g., Fig. 20) are multiplied by abundance estimates for each size class (Fig. 12) to calculate abundance by age.

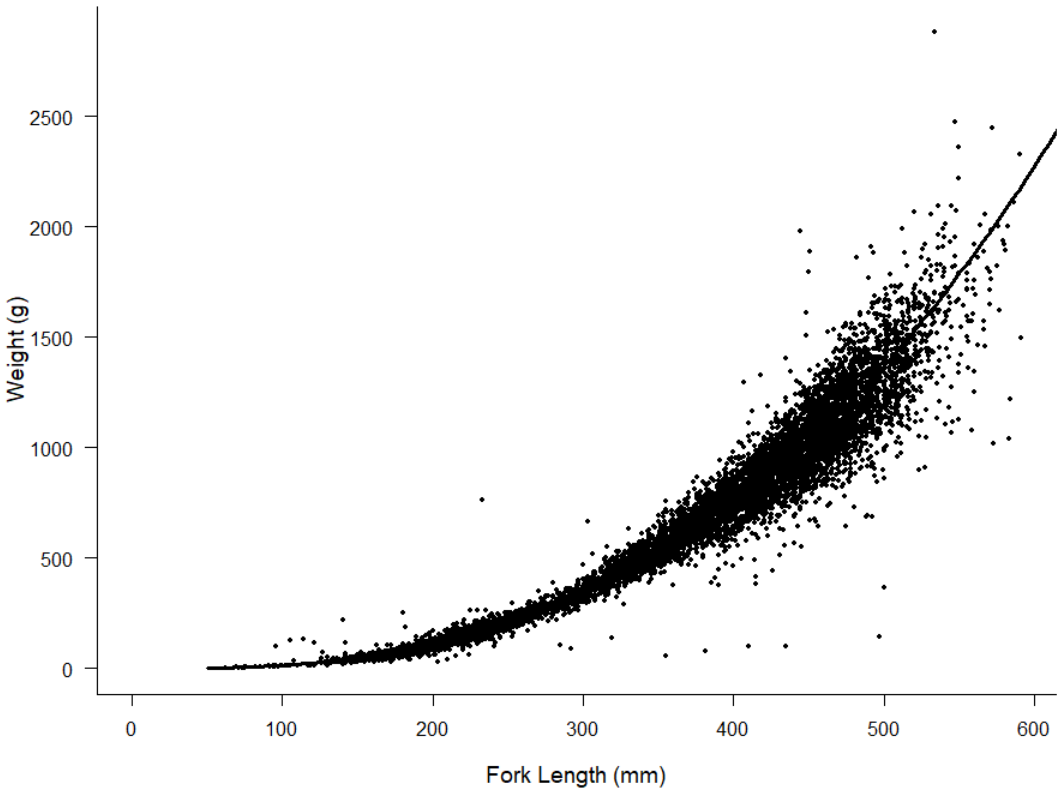

Figure 23. Length-weight relationship for Rainbow Trout using all length-weight observations from the Bow River (n=9191).

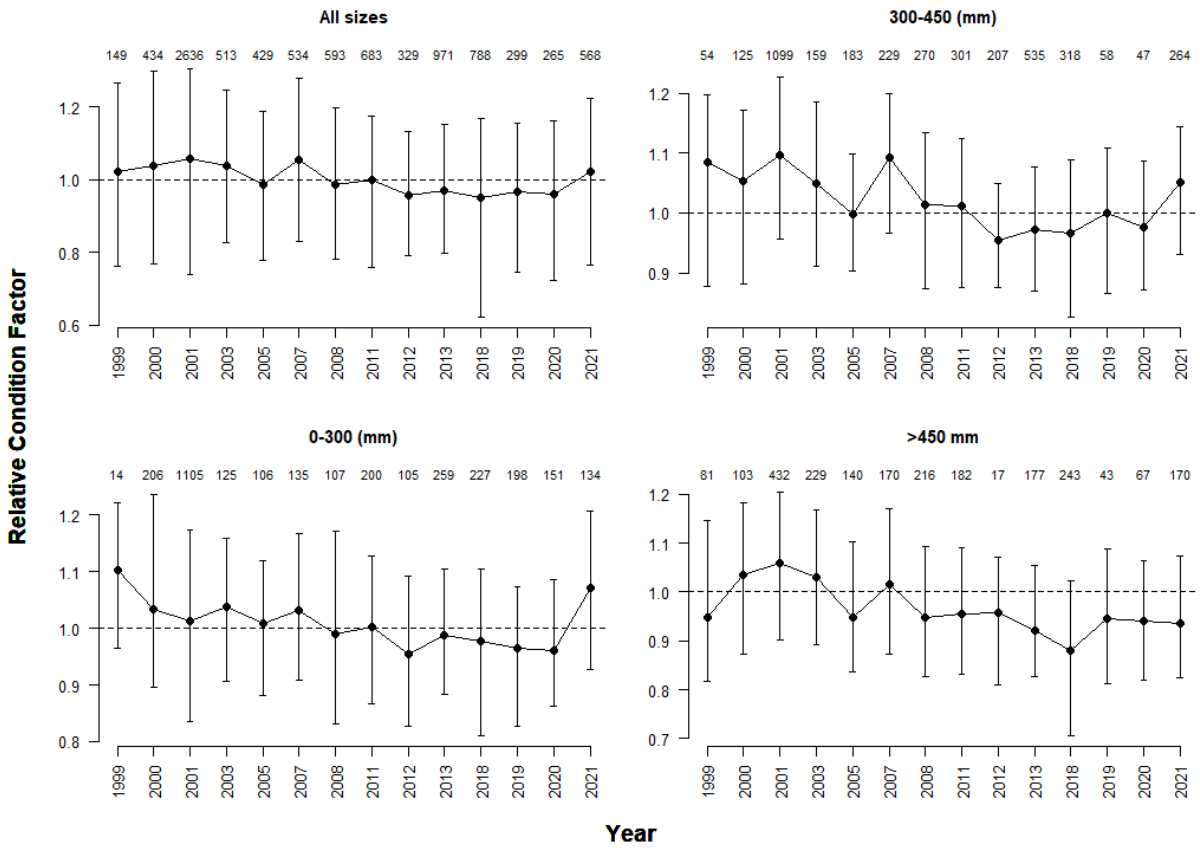

Figure 24. Relative condition factor for Rainbow Trout by year and size class using all length-weight observations (n=9191). Points and error bars denote the median and 80% credible intervals, respectively. Numbers at the top of each panel show the sample size.

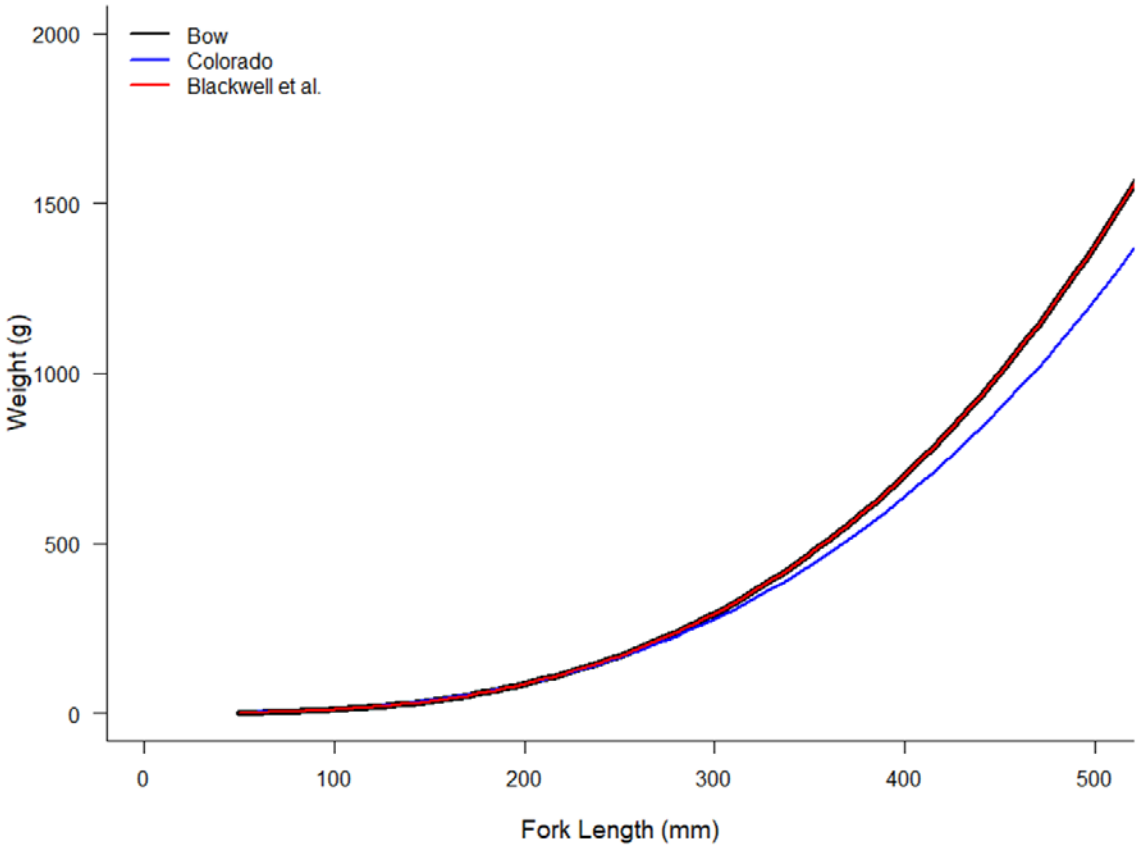

Figure 25. Comparison of Rainbow Trout length-weight relationships based on data from the Bow River (black line), populations from lotic habitats (red line, Blackwell et al. 2000), and from the Glen Canyon tailwater on the Colorado River (blue line).

Appendix A.1 Workflow to for Closed Population Model, Trend Model, and Growth Model

This appendix provides brief descriptions of the workflow needed to estimate abundance, trends in abundance, and length-at-age from the Bow River electrofishing data. Inputs data, R scripts, and WinBUGS programs to estimate annual abundance and the interannual trend are stored in the directory 'BT-CP'. Results from the abundance modelling are saved in the Output subdirectory. Length-at-age model inputs, R scripts, and the WinBUGS program are stored in the directory 'VB'. The names of these directories and their organization can easily be modified but requires making changes to the paths in some R scripts.

The workflow to run the closed population model is outlined in Figure A.1 and described below.

1. The electrofishing data is the key input to the model, and is generically referred to as EF_Data.xlsx in figure A1. The current modelling is based on BowR_Data _Master_Feb2023_JK.xlsx in the EFFishData_AllYears sheet.

2. The R script Across_Year_Site.R reads in the electrofishing file and generates a series of text files that provide lists of across-year recaptures, across-bank recaptures, and across-site recaptures (for all species). The latter list, saved in the Across_Site_Recaps.txt file is required as part of the model data-generating process and will be used by Build_Mij.R.

3. The user specifies the number of size classes to be modelled by selecting the appropriate size-class input file. New versions of these files are easily created if a different size class structure is desired. Year_Indexing.txt, which specifies the years to be modelled and the availability of mark-recapture and one-pass data for each year is another required input file.

4. The R script Build_Mij.R creates the following species-specific model input files:

    a. Catch_RNTR_SZ6.txt. A list of year-sites with the number of unmarked fish captured and new marks applied for each size class and pass from mark-recapture sites only. Note that mark-recapture sites where there were no marked releases of the specified species prior to the last pass are treated as one-pass sites, and not included in this list.
    b. MarkRecap_RNTR_Sz6.txt. A matrix of marks releases and recaptures by year, site, size class and pass.
    c. OnePass+RTNR_Sz6.txt A list of year-sites with the catch of unmarked fish by size class at one-pass sites.

5. The R script Model.R reads in the model input files created in step 4, as well Year_Indexing.txt and Sz6.txt, and creates the data input list for the WinBUGS closed population model Mysp.bug. This script also sets the initial conditions for the model and specifies the model parameters and other variables that will be saved in the output. The script then calls Mysp.bug and saves the output in the /output subdirectory after the model has completed execution.

6. Saved output from the WinBUGS model includes the samples from the posterior distributions (Mysp_RNTR_Sz6_post.out), summary statistics of the posterior distributions (Mysp_RNTR_Sz6_sum.out), and the deviance information criteria scores (Mysp_RNTR_Sz6_dic.out) which can be useful for comparing models.

7. The R script Plot_Model.R reads in the saved WinBUGS output, as well as some other data files (Year_Indexing.txt specified by user and Site_Indexing.txt generated from Build_Mij.R) It then calls Plot_pCaps.R and Plot_Abundance.R which creates graphs of model output.

Program	Files	Action
	EF_Data.xlsx	
	↓	
Across_Year_Site.R	Across_Site_Recaps.txt	Build list of across-site recaptures
	Sz6.txt	Specify # of size classes
	Year_Indexing.txt	
	EF_Data.xlsx	
	↓	
Build_Mij.R		Specify species, create model input files
	↓	
	Catch_RNTR_Sz6.txt	
Model input files:	MarkRecap_RNTR_Sz6.txt	
	OnePass_RNTR_Sz6.txt	
	↓	
Model.R		Setup data and other conditions
(calls Mysp.bug)		for bugs model. Call bugs model
	↓	
	Mysp_RNTR_Sz6_post.out	Output from Model.R
	Mysp_RNTR_Sz6_sum.out	(saved bugs output)
	Mysp_RNTR_Sz6_dic.out	
	↘	
Plot_Model.R calls:		Read bugs output
(Plot_pCaps.R)		and create graphical output
(Plot_Abundance.R)		

Figure A.1. Workflow for closed-population modelling. See text for details.

Estimates of the interannual trend in abundance for a species and age class are calculated by a separate program and workflow outlined in Figure A.2 and described below.

1. Size-specific abundance estimates from the closed population model (e.g., Mysp_RNTR_Sz6_sum.out) are read in by Model_Trend.R. In the current example, the trend in abundance of Rainbow Trout ≥ 250 mm is used.

2. Model_Trend.R calls Trend.bug, a WinBUGS program which calculates the intercept and slope of the trend line, and the extent of process error around the trend line. The model uses the mean estimates of annual abundance and uncertainty in those abundance estimates (standard deviation) as inputs (which were saved in Mysp_RNTR_Sz6_sum.out).

3. An R script, Plot_Trend.R, is used to plot the input data (abundance and uncertainty) and the fitted trend line and its uncertainty.

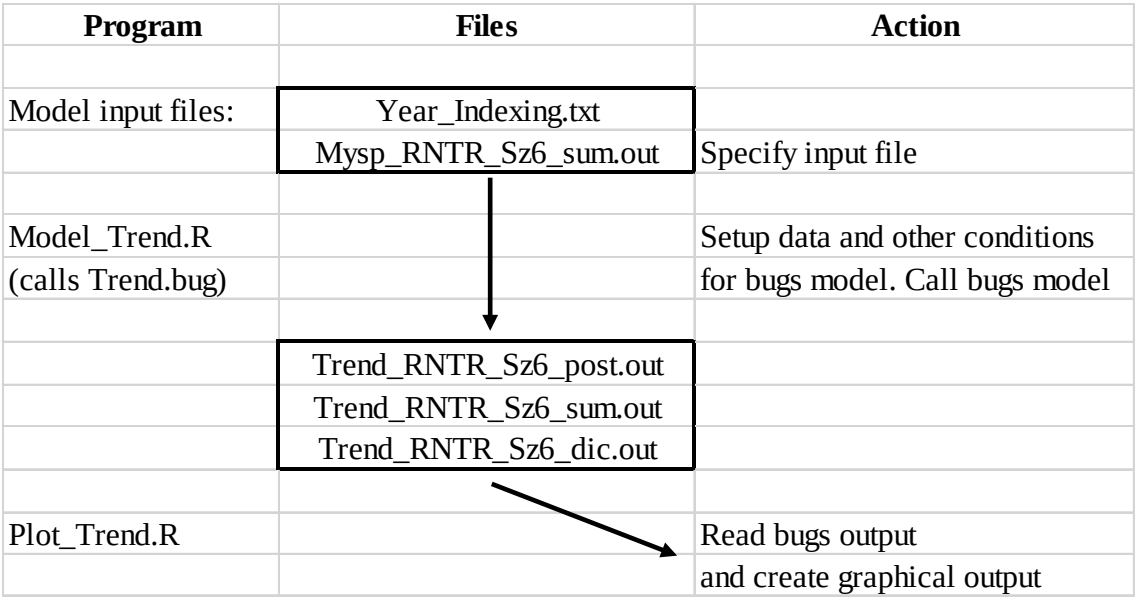

Figure A.2. Workflow for population trend modelling. See text for details.

Annual estimates of von Bertalanffy (vB) length-at-age model parameters are calculated from ageing data. The programs and workflow are outlined in Figure A.3 and described below.

1. The R script Build_Data.R reads in the ageing data and creates a species-specific model input file (e.g., RNTR.txt) which contains fields for year, age, and forklength.

2. The R script Model.R reads in the input file and creates the data input list for the VB1.bug WinBUGS program, sets the initial conditions for the model, and specifies the model parameters and other variables that will be saved in the output. The script then calls the VB1.bug model and saves the output after the model has completed execution.

3. An R script Plot_Model.R reads in the WinBUGS output and plots the data (length-at-age) and vB length-at-age models.

4. A separate R script, Prop_Age_By_Size_WithErr.R, can be used to convert abundance-by-length class into abundance-by-age class for a user selected year (DoYear). This program reads in the samples of the posteriors for the vB models (e.g., RNTR_post.out) created in step 2) and the samples of the posteriors for abundance by length class (e.g., Mysp_RNTR_Sz6_post.out). The script then calculates the abundance by age class, accounting for uncertainty in assignment of age from length from the vB models, and uncertainty in the length-class specific abundance estimates from the closed population model. The script then plots the age-specific abundance estimates.

Program	Files	Action
Build_Data.R	AgeMatData.xlsx	
	↓	Create model input file
Model input file:	RNTR.txt	
	↓	
Model.R	RNTR_post.out	Setup data and other conditions
(calls VB1.bug)	RNTR_sum.out	for bugs model. Call bugs model
	RNTR_dic.out	
	↓ ↘	
Plot_Model.R		Read bugs output
	↓	and create graphical output
	Sz6.txt, Year_Indexing.txt	
Prop_Age_By_Size_with_Err.R	Mysp_RNTR_Sz6_post.out	
	↘	
		Convert length-based abundance estimates
		into age-based abundance estimates

Figure A.3. Workflow for von Bertalanffy length-at-age modelling. See text for details.